

STUDY OF THE $\gamma p \rightarrow \pi \Delta$ (1236) REACTION
IN THE ENERGY REGION
BETWEEN 744 MeV AND 1044 MeV

By

Atsushi SASAKI*

Department of Physics, Faculty of Science, Kyoto University, Kyoto

(Received August 24, 1974)

ABSTRACT

The momentum spectra of positive and negative pions from the reaction $\gamma p \rightarrow \pi \pi N$ have been measured by a magnetic spectrometer and the photon subtraction method at the laboratory angles of 20° , 40° , 60° and 90° and at the energies of 744, 844, 944 and 1044 MeV.

Both spectra show a peak corresponding to the reaction $\gamma p \rightarrow \pi \Delta$ (1236). The differential cross sections of the reactions $\gamma p \rightarrow \pi^- \Delta^{++}$ (1236) and $\gamma p \rightarrow \pi^+ \Delta^0$ (1236) have been deduced from the obtained spectra by the analysis performed with the amplitudes for the reaction $\gamma p \rightarrow \pi \Delta$ (1236) and the phase space background.

The ratios of cross sections $\sigma(\gamma p \rightarrow \pi^+ \Delta^0(1236))/\sigma(\gamma p \rightarrow \pi^- \Delta^{++}(1236))$ at each energy are estimated to be in the range of 0.1 to 0.8 depending on the energy.

The obtained centre of mass cross sections $d\sigma/d\Omega^*(\gamma p \rightarrow \pi^- \Delta^{++}(1236))$ and $d\sigma/d\Omega^*(\gamma p \rightarrow \pi^+ \Delta^0(1236))$ have been compared with the theoretical calculations by the gauge invariant one pion exchange model with the phenomenological amplitudes for the reaction $\gamma p \rightarrow N^* \rightarrow \pi \Delta$ (1236). The theoretical calculations explain our experimental results qualitatively and show a certain contribution of the resonance $D_{13}(1525)$ to the reaction $\gamma p \rightarrow \pi \Delta$ (1236).

1. Introduction

Recently, many experimental investigations on the reaction

$$\gamma + p \rightarrow \pi + \pi + N \quad (1.1)$$

have been made.^{1~7)} In most of the counter experiments, negative pions from the reaction

$$\gamma + p \rightarrow \pi^- + \pi^+ + p \quad (1.2)$$

have been measured to identify this reaction. The reaction (1.2) has been also measured by using bubble chambers. The results of studies¹⁾ show that the cross section of the reaction (1.2) rises sharply from the $\pi \Delta$ (1236) production threshold (~ 500 MeV) and has the largest value ($\sim 80 \mu b$) around the energy of 600 MeV, then decreases gradually with the increase of photon energy.

* Now at Department of Physics, Faculty of Education, Akita University

(1.1) in the energy region of 750–1050 MeV and in the angular region of 20° – 90° have been measured by using a magnetic spectrometer system and the photon subtraction method. The obtained spectra have been analyzed in terms of the amplitudes of the reaction (1.3) and the phase space background to obtain the cross sections of the reactions (1.4) and (1.5) and the ratio r_1 . The results have been compared with theoretical calculations based on the gauge invariant one pion exchange model with the phenomenological amplitudes for the reaction (1.8).

The experimental apparatus and procedure are described in section 2 and 3, respectively. Section 4 is devoted to the procedure of data reduction. The derivation of the cross sections of the reactions (1.4) and (1.5) is given in section 5. The procedure of theoretical calculations is presented in section 6 and in the appendix. The results are discussed in section 7.

2. Experimental apparatus

2-1. Photon beam and hydrogen target

Experiment has been performed with the bremsstrahlung beam from the 1.3 GeV electron synchrotron at the Institute for Nuclear Study, University of Tokyo. The schematic layout of experimental apparatus is presented in Fig. 1. The bremsstrahlung beam was produced with electrons accelerated in the synchrotron and striking an internal copper radiator of 500 μm thick. The beam was defined by a lead collimator of 20 cm long having a circular hole of 2 cm in diameter located at 10.9 m from the radiator. Then the beam was passed through a sweep magnet and

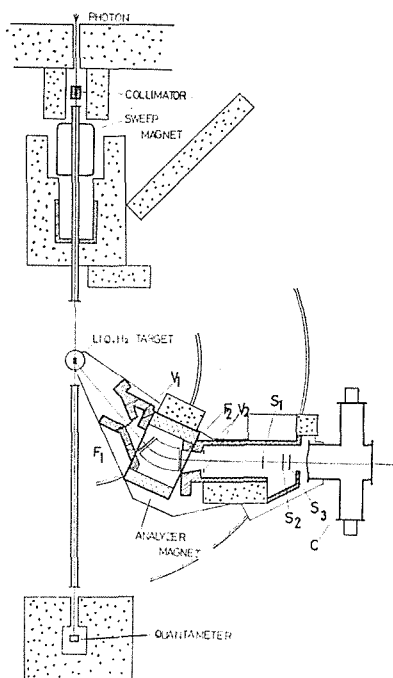


Fig. 1. Schematic layout of experimental apparatus.

led into the experimental area with an evacuated pipe. The beam profile was measured to be 3.2 cm in diameter with the method of photometry using X-ray films at the position of the liquid hydrogen target, 17.5 m from the radiator. The beam intensity was monitored continuously by a Wilson type quantameter. The integrator of the quantameter was calibrated weekly and confirmed to be within 1% in the variation of the gain. The spill time of the beam was kept within ± 1 ms around the time of a maximum magnetic field of the synchrotron and was monitored continuously by a spill monitor¹¹⁾. The liquid hydrogen was contained in a cylindrical container of 5 cm in diameter and 10 cm in length which was made of Mylar of 0.075 mm thick. A device set on the target enabled us to evacuate the liquid hydrogen from the container within a few minutes.

2-2. The pion spectrometer

The spectrometer was set on the rotating platform and consisted of an analyzing magnet, a threshold gas Čerenkov counter C , two groups of scintillation counters, one (S_1, S_2, S_3) in coincidence and the other (V_1, V_2, F_1, F_2) in veto. The parameters and functions of the counters are listed in Table 1.

The trajectories of charged particles were limited by the veto-counters. The frame-like counter V_1 was used to define the solid angle of the spectrometer. The counter V_2 was also used to define the angular acceptance of the spectrometer. The counters F_1 and F_2 were set on the pole face of the magnet so as to reject particles scattered at the pole piece of the magnet. Flexible adiabatic light guides of silicon rubber¹²⁾ were used to collect the light of the counters F_1 and F_2 through long pathes in the magnet. Each veto counter consisted of a pair of identical scintillation counters which were used in coincidence to reduce the accidental countings. A helium bag was set along the beam path of the spectrometer to reduce the effect of the multiple Coulomb scattering. The counter S_3 was placed at the focal point of the magnet and defined the momentum acceptance of the spectrometer. Pulse heights of signals of the counters S_1 and S_3 were used to distinguish protons from pions at the positive

Table 1. Counter parameters

	Distance from H_2 target	Function	Defining aperture	Thickness
Veto counters				
V_{1V}	197.9 cm	angular acceptance	± 4.0 cm, vertically	1 cm
V_{1V}	200.9 cm	angular acceptance	± 9.0 cm, horizontally	1 cm
F_1	256.6 cm	rejection of surface scattering	± 4.0 cm, vertically	1 cm
F_2	351.0 cm	rejection of surface scattering	± 4.8 cm, vertically	1 cm
V_2	408.5 cm	angular acceptance	± 15.0 cm, horizontally width height	1 cm
Telescope counters				
S_1	547.9 cm	proton rejection	27.0 cm \times 21.0 cm	0.3 cm
S_2	593.4 cm		27.0 cm \times 27.0 cm	0.3 cm
S_3	608.8 cm	momentum acceptance and proton rejection	24.0 cm \times 20.0 cm	0.6 cm
Threshold gas Čerenkov counter				
C	643.8 cm	electron rejection	24 cm \times 20 cm with the beam window of 50 cm in diameter and 6.5 mm thick Mylar	

pion run. A copper plate of 3 mm thick was placed in front of the counter S_3 to reduce the room background.

Characteristics of the magnet were investigated by a floating wire technique and with a flip coil calibrated by a NMR magnetmeter. The solid angle $\Delta\Omega$ and the momentum acceptance $\Delta p/p$ were calculated to be 2.5 msr and 0.1, respectively, by a Monte Carlo simulation taking into account of the results of floating wire measurement and field mapping.

2-3. Gas Čerenkov counter

In the present experiment, a large amount of contaminations of electrons or positrons must be eliminated. A threshold gas Čerenkov counter of Freon-12 was constructed and set on the platform at the down stream of the counter S_3 to detect electrons or positrons.

The schematic view of the Čerenkov counter is illustrated in Fig. 2. To reduce the multiple Coulomb scattering of electrons at the entrance of the counter, a beam window of 50 cm in diameter was constructed by twenty-six sheets of 0.25 mm thick polyester film¹³⁾. The counter was designed to have the horizontal and vertical acceptance of 25 cm \times 20 cm in space and $12^\circ \times 8^\circ$ in angle. The gas container was tested by applying a hydraulic pressure of 15 kg/cm² and found to be safe. The Čerenkov photons were collected through two light funnel of Winston-Hinterberger type¹⁴⁾ and detected by two phototubes (RCA 4522) attached to the quartz glass window of 35 mm thick. The accepting angle of the light funnel was designed to be 12° .

The counter was operated at the pressure of 6 kg/cm² and at the temperature

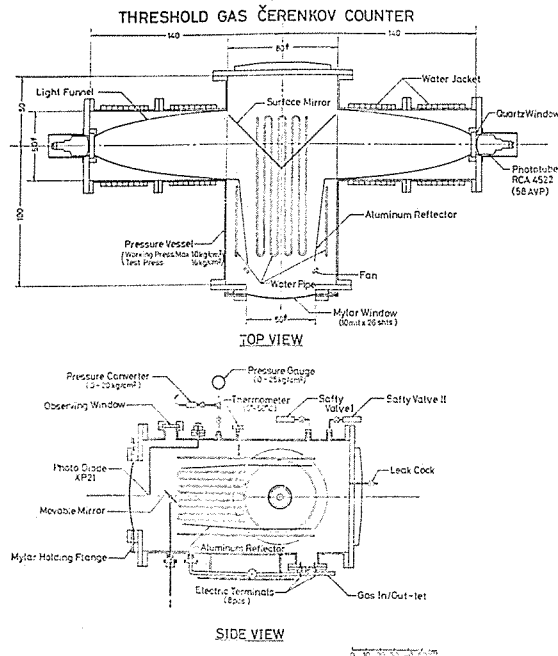


Fig. 2. Schematic view of the gas Čerenkov counter.

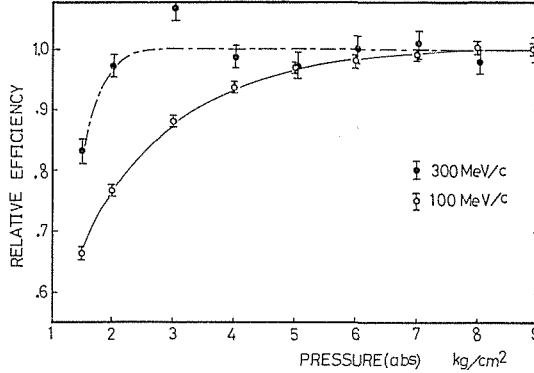


Fig. 3. Detection efficiency of the gas Čerenkov counter which is defined Ne/N (see the text) and normalized to 1.0 at the pressure of 9 kg/cm².

of 37°C during the experiment. The threshold momentum for pion and muon is 1200 and 910 MeV/c, respectively. The results of measurement show that the detection efficiency of the counter is higher than 98 % for 150 MeV/c electrons and 99 % for 300 MeV/c electrons as shown in Fig. 3.

3. Experimental procedure

3-1. Yield of charged particles

The counters S_1 , S_2 and S_3 are used in coincidence ($S=S_1 \cdot S_2 \cdot S_3$). The signals of the counters V_1 , V_2 , F_1 and F_2 are summed up ($X=V_1+V_2+F_1+F_2$). When the countings of S and $S \cdot X$ are written as Ns and Nsx , respectively, the countings of available charged particles $N (=Ns\bar{x})$ is obtained as following,

$$N(=Ns\bar{x})=Ns-Nsx. \quad (3.1)$$

The yield Ns contains the yields due to pions and electrons at the negative pion runs and the yields due to pions, positrons and protons at the positive pion runs.

3-2. Subtraction of electron yields

The yield of electrons or positrons $Ne (=Ncs\bar{x})$ was obtained from the coincidence countings Ncs and $Ncsx$ of the Čerenkov counter with S and $S \cdot X$, respectively,

$$Ne(=Ncs\bar{x})=Ncs-Ncsx. \quad (3.2)$$

The yield of electrons or positrons Ne was subtracted from the yield of charged particles N . An example of electron yield is shown in Fig. 4. The yield due to electrons was about five times of the yield due to pions at the laboratory angle of 20° and momentum of 100 MeV/c. Most of the electrons were created by low energy photons and eliminated through the procedure of photon subtraction. Thus the background due to the inefficiency of Čerenkov counter was negligibly small in most of the runs.

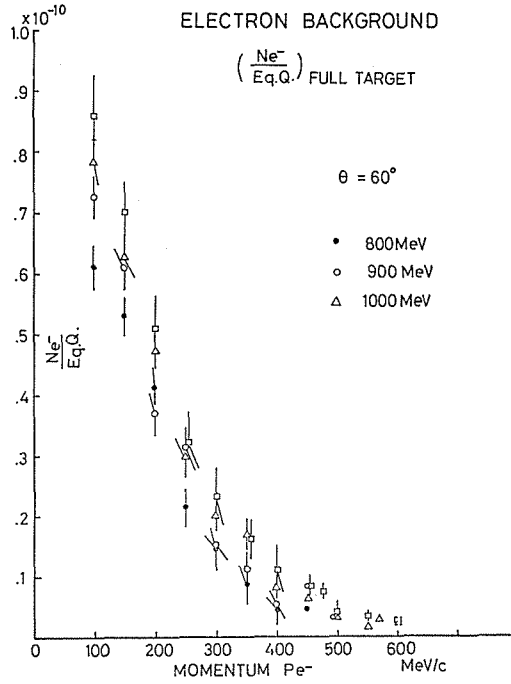


Fig. 4a. Examples of electron yields.

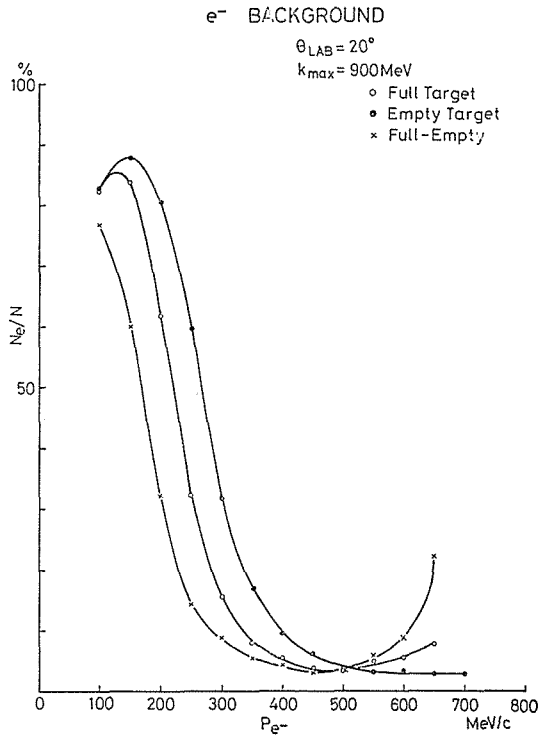


Fig. 4b. Examples of the fraction of electron yields.

3-3. Subtraction of proton yields.

At the positive pion run the coincidence event S was rejected by the signals of counter S_1 with a sufficiently large pulse height compared to those of pions. Thus the yields due to protons were eliminated partly by the fast electronic logic. For the complete elimination of proton yields, the pulse height of signals of counter S_3 recorded on the pulse height analyzer was used. A typical example of pulse height distribution is shown in Fig. 5.

The procedure of proton subtraction is as follows. At first, "cut off channel" was defined for each momentum. Below this channel, the proton contamination was negligibly small compared to the pion yield ($\leq 1\%$, see Fig. 5). All the events lying below the cut off channel were considered to be pions and positrons. Then assuming a Landau distribution on the pulse height distribution, the number of pions and positrons above the cut off channel was estimated and found to be about 15% of those below the cut off channel at 700 MeV/c.

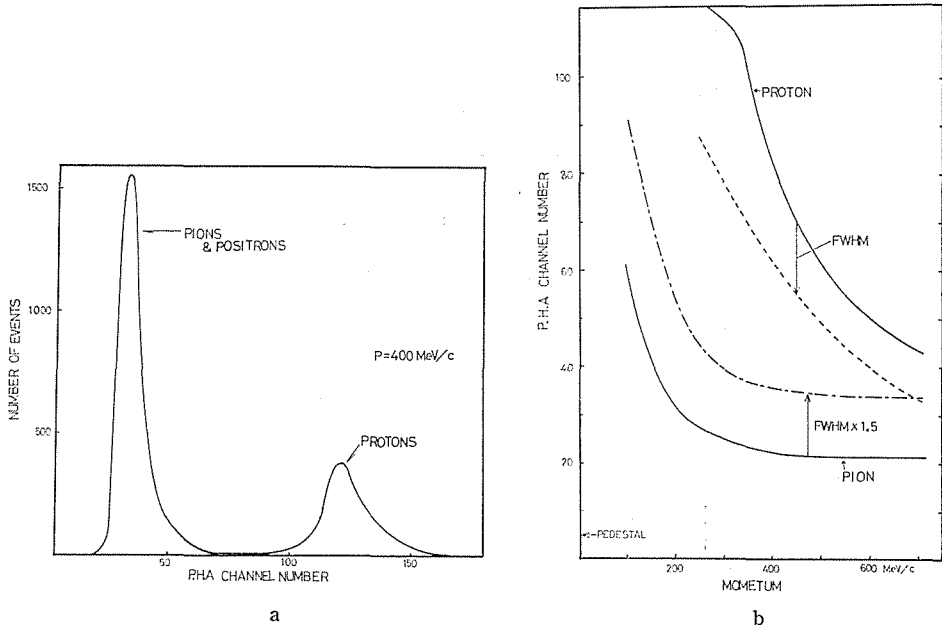


Fig. 5a. Typical pulse height distribution of the counter S_3 .

Fig. 5b. Peak channels of the counter S_3 due to pions and protons. The dashed curve represent the cut off channel (see the text).

3-4. Subtraction of empty target yield.

The yields from the materials other than liquid hydrogen was subtracted in a well established manner by the empty target run. In most of the runs, the empty target yields were about 20% of that for full target.

3-5. Data collection

A typical momentum spectrum of positive pions obtained after the photon subtraction between the photon energies of 800 and 900 MeV is shown in Fig. 6. The spectrum below 450 MeV corresponds to the reaction $\gamma + p \rightarrow \pi^+ + \pi + N$ and

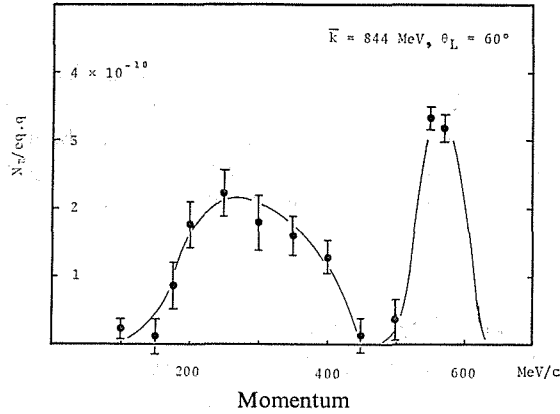


Fig. 6. Typical momentum spectra of positive pions obtained after the photon subtraction between the photon energies of 800 and 900 MeV.

the spectrum above 450 MeV/c corresponds to the reaction $\gamma + p \rightarrow \pi^+ + n$. Thus the positive pion yield due to the reaction $\gamma + p \rightarrow \pi^+ + \pi + N$ is separated well enough from the one due to the reaction $\gamma + p \rightarrow \pi^+ + n$ when the photon subtraction with the energy width of 100 MeV is performed.

A measurement of the cross section of the reaction $\gamma + p \rightarrow \pi^+ + n$ was performed to confirm the reliability of the spectrometer system before the data collection and found to be in good agreement with the existing data within the statistical error. The check of the spectrometer system was performed periodically during

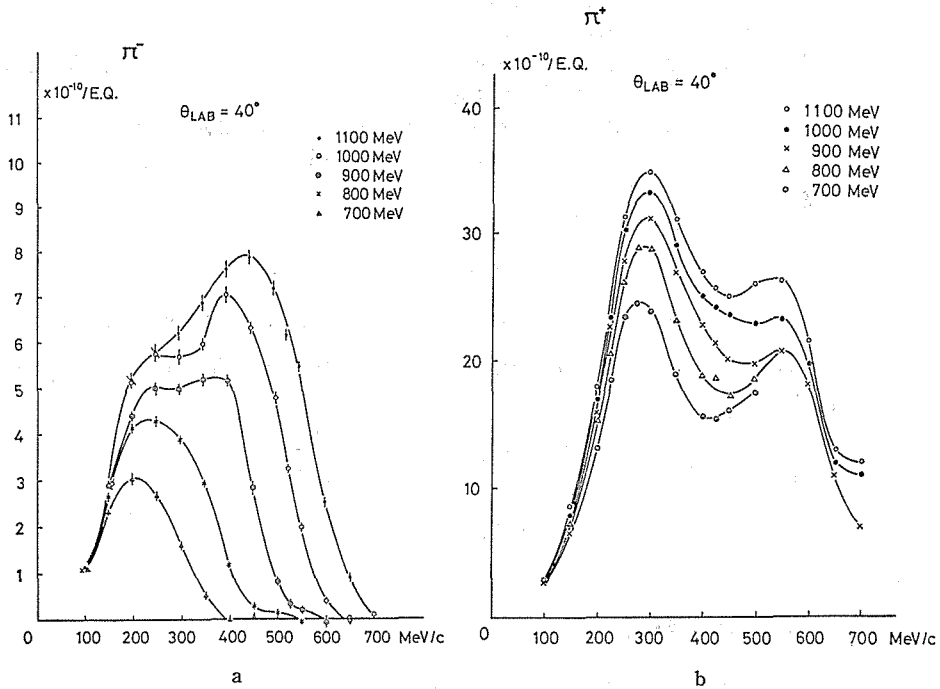


Fig. 7. Examples of yield curves of (a) negative pions and (b) positive pions.

the experiment.

The yields of positive and negative pions were measured as a function of momentum from 100 MeV/c with a step of 25 or 50 MeV/c. The data were collected at the laboratory angles of 20°, 40° and 60° for the bremsstrahlung having the maximum energies of 700, 800, 900, 1000 and 1100 MeV. Moreover, the positive pions were measured at the angle of 90° for the maximum energies of 900, 1000 and 1100 MeV. The typical curves are shown in Fig. 7.

4. Data reduction

4-1. Formula for the laboratory cross section

The observed pion yield N_π per equivalent quanta is expressed by the followings

$$N_\pi = \eta \cdot \int_{K_0}^K \frac{d^2\sigma}{dpd\Omega} \cdot \Delta\Omega \cdot \Delta p \cdot N_H \cdot \frac{B(K, k)}{k} dk + \eta \cdot \xi \cdot \frac{d\sigma_s}{d\Omega} \cdot \Delta\Omega \cdot \frac{\partial k_r}{\partial p} \cdot \Delta p \cdot N_H \cdot \frac{B(K, k_r)}{k_r} \quad (4.1)$$

where the first and second terms represent the contribution from the reaction $\gamma + p \rightarrow \pi + \pi + N$ and $\gamma + p \rightarrow \pi^+ + n$, respectively, and

$\frac{d^2\sigma}{dpd\Omega}$ = the cross section of the reaction $\gamma p \rightarrow \pi\pi N$

$\eta, \Delta\Omega, \Delta p$ = detection efficiency, solid angle and momentum acceptance of the spectrometer, respectively

N_H = number of target protons

K = maximum energy of bremsstrahlung

K_0 = minimum photon energy to produce two pions one of which can be detected by the spectrometer

$B(K, k)/k$ = number of photons with the energies between k and $k + dk$, where $B(K, k)$ is a bremsstrahlung form factor

$\xi = \begin{cases} 0, & \text{for negative pion run} \\ 1, & \text{for positive pion run} \end{cases}$

$\frac{d\sigma_s}{d\Omega}$ = cross section of the reaction $\gamma p \rightarrow \pi^+ n$ at the responsible photon energy k_r , when the π^+ is observed by the spectrometer.

According to eq. (4.1), the cross section $d^2\sigma/dpd\Omega$ at the energies between K_1 and K_2 ($K_2 < K_1$) is given by

$$\frac{d^2\sigma}{dpd\Omega} = \frac{(Y_{K_1} - Y_{K_2}) - \xi \cdot \frac{\partial k_r}{\partial p} \cdot R(K_1, K_2, k_r) \cdot \frac{d\sigma_s}{d\Omega}}{\int_{K_0}^{K_1} R(K_1, K_2, k) dk} \quad (4.2)$$

where

$$Y_K = N_\pi / N_H \Delta\Omega \Delta p \eta$$

$$R(K_1, K_2, k) = \frac{B(K_1, k) - B(K_2, k)}{k}$$

By using the observed yields, the laboratory cross sections $d^2\sigma/dpd\Omega$ of the reaction (1.1) were obtained according to the eq. (4.2) at the mean photon energies of 744, 844, 944 and 1044 MeV. The dependence of cross sections on the momentum is called "momentum spectrum", here after. The counting efficiency of the spectrometer η and the second term in the numerator of right side of eq. (4.2) were evaluated numerically. For the evaluation of η , the decay and absorption of pions were taken into account.

4-2 Decay correction

The observed yield Y_0 is related to the yield Y of pions which are produced in the target and emitted in the angular and momentum acceptance of the spectrometer,

$$Y_0 = (\alpha + \beta) \cdot Y + Y' \quad (4.3)$$

where

α = the fraction of the acceptable pions which are observed before decaying into muons.

β = the fraction of the acceptable pions which are observed after decayed into muons.

Y' = yield of muons from the pions which are emitted out of the angular and momentum acceptance of the spectrometer.

The eq. (4.3) gives following equation,

$$Y = Y_0 \cdot \frac{1 - \gamma}{\alpha + \beta} \quad (4.4)$$

where

$$\gamma = Y' / Y_0.$$

Monte Carlo calculations were performed to obtain the values of β and γ . The values of γ were found to be about 0.15 and 0.1 for 100 and 200 MeV/c, respectively. For the momenta above 200 MeV/c, γ was nearly constant and evaluated to be about 0.1. The value of β was about 0.08 for 300 MeV/c. A typical

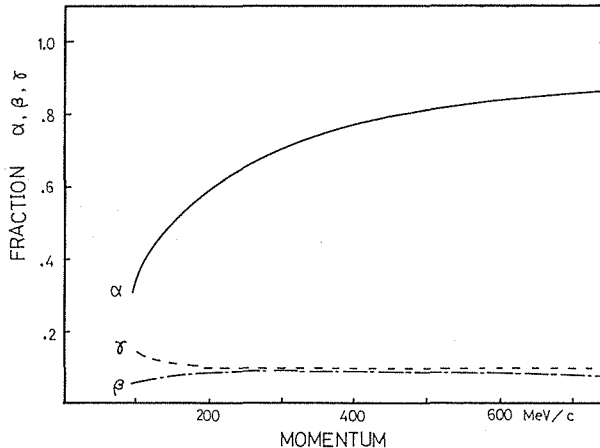


Fig. 8. Results of the calculations for the correction factors α , β and γ for the decay correction.

result of calculation for α , β and γ are shown in Fig. 8. The correction for the decay effect of pions were about 100 %, 30 % and 4 % for 100, 200 and 300 MeV/c, respectively, and were negligibly small for higher momenta. The accuracy of these calculations were about 10 % due to the statistical errors of Monte Carlo simulation.

4-3. Correction due to the nuclear absorption

The materials taken into account in the calculation of nuclear absorption are Mylar wall of liquid hydrogen target, air and helium, counters S_1 and S_2 and the copper plate. For the calculation, existing data of elastic and inelastic pion nuclei interaction cross sections are used¹⁵⁾.

Some of pions interact inelastically with the carbon nuclei in the counter S_1 and S_3 . Due to these inelastic interactions, those pions are detected as protons in the positive pion run. Corrections due to this effect were also taken into account.

The total corrections due to the nuclear absorption were found to be about 6 % for both positive and negative pions at the momentum of 300 MeV/c as shown in Fig. 9. The errors of these corrections were due to the accuracy of the $A^{2/3}$ law and the experimental errors of data of pion-nuclei cross sections and estimated to be about 10 % of corrections.

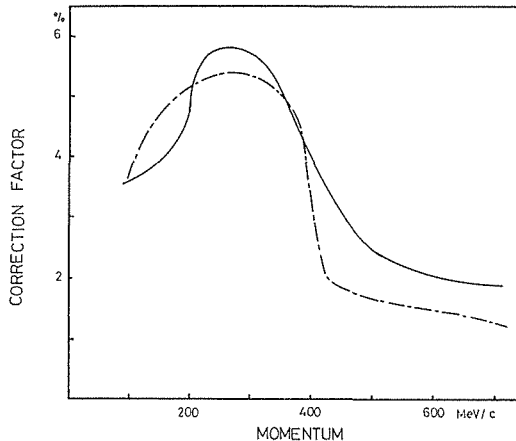


Fig. 9. Correction factors for the nuclear absorption. Solid curve: for negative pions, dashed curve: for the positive pions.

4-4 Correction for the contamination from single pion photoproduction

As there remains a small number of low energy photons ($k < K_2$) in the subtracted photon spectrum^{7,24)}, $R(K_1, K_2, k)$, the effect of second term in the numerator of right side of eq. (4.2) must be taken into account in the positive pion run. This term was calculated to be about 3 % typically.

5. Cross section of $\gamma p \rightarrow \pi \Delta(1236)$

5-1. Fitting formula

The obtained momentum spectra were analyzed by assuming pions produced through the process (1.3) and a direct process (a three body phase space background). The spectrum is described by,

$$\frac{d^2\sigma^\pm}{dp_1 d\Omega_1} = \frac{p_1^2}{2E_1} \int \frac{d^3p_2}{2E_2} \cdot \frac{d^3p_3}{2E_3} \cdot \delta^4(p_i - p_f) \cdot \{ |A_0^\pm|^2 + |A_1^\pm|^2 + |A_1^{\pm*}|^2 + 2\text{Re}(A_0^\pm \cdot A_1^{\pm*}) + 2\text{Re}(A_0^\pm \cdot A_2^{\pm*}) + 2\text{Re}(A_1^\pm \cdot A_2^{\pm*}) \}, \quad (5.1)$$

where

(E_i, p_i) , $i=1,2,3$ =four momentum of observed pion (π_1), un observed pion (π_2) and the nucleon, respectively,

A_0 =amplitude related to the pion from the phase space background,
 A_1, A_2 =amplitude related to the recoil pion of the quasitwo body process $\gamma p \rightarrow \pi d(1236)$ and the decay pion from $d(1236)$, respectively.

The superscript (\pm) denotes the charge state of observed pion (π_1). The amplitudes A_1 and A_2 are given by

$$\begin{aligned} A_1 &= a_1 e^{i\delta_2} \sin \delta_2 / \sqrt{W_0 \Gamma} \\ A_2 &= a_2 e^{i\delta_1} \sin \delta_1 / \sqrt{W_0 \Gamma} \\ \delta_j &= \tan^{-1} \frac{W_0 \Gamma}{W_0 - W_j} \quad (j=1, 2) \end{aligned} \quad (5.2)$$

where

W_0, Γ =the mass and width¹⁶⁾ of $d(1236)$, respectively,
 W_j =the invariant mass of j -th pion and nucleon.

5-2 Isospin amplitude and fitting procedure

The amplitudes a_1^\pm and a_2^\pm are decomposed as

$$\begin{aligned} a_1^- &= \sqrt{\frac{1}{2}} T_1(\theta_1) + \sqrt{\frac{2}{5}} T_3(\theta_1), \\ a_1^+ &= \sqrt{\frac{1}{6}} T_1(\theta_1) - \sqrt{\frac{8}{15}} T_3(\theta_1), \\ a_2^- &= \sqrt{\frac{1}{3}} \left\{ \sqrt{\frac{1}{6}} T_1(\theta_2) - \sqrt{\frac{8}{15}} T_3(\theta_2) \right\}, \\ a_2^+ &= \left\{ \sqrt{\frac{1}{2}} T_1(\theta_2) + \sqrt{\frac{2}{5}} T_3(\theta_2) \right\} + \sqrt{\frac{1}{3}} \left\{ -\sqrt{\frac{1}{3}} T_1(\theta_2) + \sqrt{\frac{1}{15}} T_3(\theta_2) \right\}, \end{aligned} \quad (5.3)$$

where θ_1 and θ_2 are the azimuthal angles of π_1 and π_2 , respectively. The amplitudes T_1 and T_2 represent the s-channel isospin amplitudes with $I=\frac{1}{2}$ and $\frac{3}{2}$, respectively. The first and second terms appeared in the decomposition of a_2^\pm correspond to the decay π^+ from $d^{++}(1236)$ and $d^+(1236)$, respectively.

The amplitudes A_0^\pm, T_1 and T_3 were determined so that the eq. (5.1) reproduce the observed momentum spectra of both positive and negative pions at each photon energy and laboratory angle by a least square method. In the fitting procedure, the amplitude T_3 was treated as a real number because it was plausible that resonances with $I=\frac{3}{2}$ were scarcely photoproduced below 1 GeV. The amplitudes

$T_i(\theta_1)$ and $T_i(\theta_2)$ were treated as different from each other. Moreover, the amplitudes $T_i(\theta_2)$ were treated as independent on the angle θ_2 for the actual fitting procedure. The parameters fitted are four real numbers, A_0^+ , A_0^- , $T_3(\theta_1)$ and $T_3(\theta_2)$ and two complex numbers, $T_1(\theta_1)$ and $T_1(\theta_2)$.

The interference terms $2\text{Re}(A_0^+ \cdot A_1^+)$ and $2\text{Re}(A_0^+ \cdot A_2^+)$ in the eq. (5.1) were ignored in the fitting procedure. The cross terms between different charge states were excluded for the positive pion spectrum. The effect of the reactions $\gamma p \rightarrow \rho N$ and $\gamma p \rightarrow \pi\pi N$ were not taken into account due to their small cross sections in our energy regions.

The laboratory cross sections $d^2\sigma/dpd\Omega(\gamma p \rightarrow \pi\Delta(1236))$ of the reactions (1.4) and (1.5) were calculated by using the eq.(5.1) with only the term $|A_1^+|^2$ which was given by the obtained values of $T_1(\theta_1)$ and $T_3(\theta_1)$.

The differential cross sections $d\sigma/d\Omega(\gamma p \rightarrow \pi\Delta(1236))$ were calculated by integrating the cross sections $d^2\sigma/dpd\Omega(\gamma p \rightarrow \pi\Delta(1236))$ over the momentum. The centre of mass cross sections $d\sigma/d\Omega^*(\gamma p \rightarrow \pi\Delta(1236))$ were obtained by using the value of Jacobian at the momentum p_1 which corresponds to the invariant mass $W_2=1236$ MeV.

6. Theoretical calculation of cross sections

6-1 Amplitudes for the reaction $\gamma p \rightarrow \pi\Delta$

Several resonances below 1.1 GeV which can decay into $\pi\Delta(1236)$ are listed in Table 2. The total cross sections of the reaction (1.1) through these resonances were calculated by using the photoexcitation amplitudes presented by Walker¹⁷⁾ with the assumption that the $\pi\pi N$ decay¹⁸⁾ occurs through the process $N^* \rightarrow \pi\Delta(1236) \rightarrow \pi\pi N$ and the calculated values are also listed in Table 2.

The resonance amplitudes corresponding to the reactions (1.8) and (1.9) are treated coherently[†] with the amplitudes of gauge invariant one pion exchange model⁸⁾ in this section. The total s-channel isospin amplitudes T^1 and T^3 corresponding to isospin $I=\frac{1}{2}$ and $\frac{3}{2}$, respectively, are presented as

$$T^1 = B^1 + R^1$$

Table 2. Resonances photoproduced below 1100 MeV

Name J^p	Mass (MeV)	Resonance energy (MeV)	Multipolarity of photon J' Name	Relative ang. momentum between π & Δ L'	$\sigma(\gamma p \rightarrow N^* \rightarrow \pi^- \Delta^{++})$ μb
$P_{11} \frac{1^+}{2}$	1460	650	1 M1	1	0.4
$D_{13} \frac{3^+}{2}$	1525	760	1 E1 2 M2	0, 2	21
$S_{11} \frac{1^+}{2}$	1560	780	1 E1	2	0.5
$F_{15} \frac{5^+}{2}$	1688	1050	2 E2 3 M3	1, 3	6
$D_{15} \frac{5^-}{2}$	1690	1050	2 M2 3 E3	2, 4	0.7

[†] See ref.19 in which the s-channel resonances are treated differently from the present procedure.

$$T^3 = B^3 + R^3 \quad (6.1)$$

where

B^1, B^3 = isospin amplitude of gauge invariant one pion exchange terms for $I = \frac{1}{2}$ and $\frac{3}{2}$, respectively

R^1, R^3 = resonance amplitude corresponding to the reaction $\gamma p \rightarrow N^* \rightarrow \pi d(1236)$ with isospin $I = \frac{1}{2}$ and $\frac{3}{2}$, respectively.

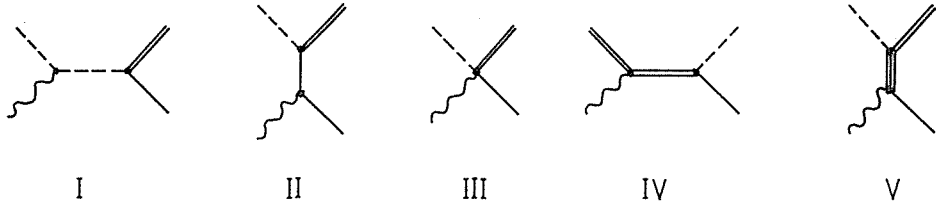


Fig. 10. Feynman diagrams which correspond to the reaction $\gamma p \rightarrow \pi d(1236)$. Graphs I~IV present the gauge invariant OPE terms⁹⁾. Graph V correspond to the reaction $\gamma p \rightarrow N^* \rightarrow \pi d(1236)$.

We present the amplitudes of the reaction (1.4) by H^I, H^{II}, H^{III} and H^{IV} corresponding to the each graph of gauge invariant one pion exchange model (see Fig. 10). Then the amplitudes B^1 and B^3 are decomposed as follows,

$$B^1 = \frac{\sqrt{2}}{3} (-H^I + 3H^{II} - H^{III} + 4H^{IV})$$

$$B^3 = \frac{\sqrt{10}}{3} (-H^I - H^{III} + H^{IV}). \quad (6.2)$$

The amplitudes for the reactions (1.4), (1.5) and $\gamma p \rightarrow \pi^0 d^+(1236)$ are given by

$$T^{++} = \sqrt{\frac{1}{2}} T^1 + \sqrt{\frac{2}{5}} T^3$$

$$T^{+-} = -\sqrt{\frac{1}{3}} T^1 + \sqrt{\frac{1}{15}} T^3$$

$$T^0 = \sqrt{\frac{1}{6}} T^1 - \sqrt{\frac{8}{15}} T^3. \quad (6.3)$$

The resonance amplitudes R^1 and R^3 are expanded in multipoles and then the cross sections of the reaction (1.3) are calculated by using the phenomenological amplitudes for each resonance. The multipole expansion of the amplitude R was performed in terms of helicity amplitudes and was given in the appendix.

6-2 Numerical calculation of cross sections

The resonances $P_{11}(1460)$, $D_{13}(1525)$, $S_{11}(1550)$, $F_{15}(1688)$ and $D_{15}(1670)$ were taken into account in the numerical calculations. Parameters used are listed in Table 3. The helicity amplitudes of the reaction (1.4) for the gauge invariant one pion exchange terms given by Locher and Sandhas²⁰⁾ were used for the calculations.

Table 3. Parameters for the phenomenological amplitudes

Resonance	Parameters	Values of parameters	Restriction taken into account	Phase angle									
P_{11}	M	$M_{11}^+ = -1.0$		-60°									
D_{13}	<table border="1" style="display: inline-table; vertical-align: middle;"> <tr> <td>$J' \backslash L'$</td> <td>0</td> <td>2</td> </tr> <tr> <td>1</td> <td>$\alpha_{13}^- \cdot E_{13}^-$</td> <td>$\beta_{13}^- \cdot E_{13}^-$</td> </tr> <tr> <td>2</td> <td>$\alpha_{13}^- \cdot M_{13}^-$</td> <td>$\beta_{13}^- \cdot M_{13}^-$</td> </tr> </table>	$J' \backslash L'$	0	2	1	$\alpha_{13}^- \cdot E_{13}^-$	$\beta_{13}^- \cdot E_{13}^-$	2	$\alpha_{13}^- \cdot M_{13}^-$	$\beta_{13}^- \cdot M_{13}^-$	$E_{13}^- = 7.9$ $\alpha_{13}^- = 1$ $\beta_{13}^- = 0$	$M_{13}^- = E_{13}^- / \sqrt{3}$	-28°
$J' \backslash L'$	0	2											
1	$\alpha_{13}^- \cdot E_{13}^-$	$\beta_{13}^- \cdot E_{13}^-$											
2	$\alpha_{13}^- \cdot M_{13}^-$	$\beta_{13}^- \cdot M_{13}^-$											
S_{11}	E_{11}^+	$E_{11}^+ = 1.0$		-23°									
F_{15}	<table border="1" style="display: inline-table; vertical-align: middle;"> <tr> <td>$J' \backslash L'$</td> <td>1</td> <td>3</td> </tr> <tr> <td>2</td> <td>$\alpha_{15}^+ \cdot E_{15}^+$</td> <td>$\beta_{15}^+ \cdot E_{15}^+$</td> </tr> <tr> <td>3</td> <td>$\alpha_{15}^+ \cdot M_{15}^+$</td> <td>$\beta_{15}^+ \cdot M_{15}^+$</td> </tr> </table>	$J' \backslash L'$	1	3	2	$\alpha_{15}^+ \cdot E_{15}^+$	$\beta_{15}^+ \cdot E_{15}^+$	3	$\alpha_{15}^+ \cdot M_{15}^+$	$\beta_{15}^+ \cdot M_{15}^+$	$E_{15}^+ = 4.5$ $\alpha_{15}^+ = 1$ $\beta_{15}^+ = 0$	$M_{15}^+ = E_{15}^+ / \sqrt{2}$	0°
$J' \backslash L'$	1	3											
2	$\alpha_{15}^+ \cdot E_{15}^+$	$\beta_{15}^+ \cdot E_{15}^+$											
3	$\alpha_{15}^+ \cdot M_{15}^+$	$\beta_{15}^+ \cdot M_{15}^+$											
D_{15}	<table border="1" style="display: inline-table; vertical-align: middle;"> <tr> <td>$J' \backslash L'$</td> <td>2</td> <td>4</td> </tr> <tr> <td>2</td> <td>$\alpha_{15}^- \cdot M_{15}^-$</td> <td>$\beta_{15}^- \cdot M_{15}^-$</td> </tr> <tr> <td>3</td> <td>$\alpha_{15}^- \cdot E_{15}^-$</td> <td>$\beta_{15}^- \cdot E_{15}^-$</td> </tr> </table>	$J' \backslash L'$	2	4	2	$\alpha_{15}^- \cdot M_{15}^-$	$\beta_{15}^- \cdot M_{15}^-$	3	$\alpha_{15}^- \cdot E_{15}^-$	$\beta_{15}^- \cdot E_{15}^-$	$M_{15}^- = 1.9$ $\alpha_{15}^- = 1$ $\beta_{15}^- = 0$	$E_{15}^- = M_{15}^- / \sqrt{2}$	0°
$J' \backslash L'$	2	4											
2	$\alpha_{15}^- \cdot M_{15}^-$	$\beta_{15}^- \cdot M_{15}^-$											
3	$\alpha_{15}^- \cdot E_{15}^-$	$\beta_{15}^- \cdot E_{15}^-$											

In the calculations followings were assumed or introduced.

- 1) The resonances $D_{13}(1525)$, $F_{15}(1688)$ and $D_{15}(1670)$ are photoexcited only through the initial states with helicity $\pm \frac{3}{2}$ (see appendix).
- 2) The angular momentum of pion of the reaction $\gamma p \rightarrow \pi \Delta(1236)$ was restricted to be $L'=0$ for $D_{13}(1525)$, $L'=1$ for $F_{15}(1688)$ and $L'=2$ for $D_{15}(1670)$, respectively.
- 3) Constant phase factors $e^{i\phi}$ were introduced for the resonance amplitudes. Values of the phase angles ϕ are chosen so that the interference between the amplitudes R^i and B^i becomes largest at the energy^{††} of 600 MeV and listed in Table 3.
- 4) The width of $\Delta(1236)$ was treated energy dependently¹⁶⁾.
- 5) A form factor $e^{\lambda(t-\mu^2)}$ is introduced at the vertices $\pi N \Delta$ and $\pi N^* \Delta$, where t is the momentum transfer squared, μ is the pion mass and λ is a parameter^{†††} and taken to be $\lambda=0.8$ (GeV/c)⁻².

7. Result and discussion

7-1. Result of the experiment

The obtained momentum spectra $d^2\sigma/dpd\Omega$ of positive and negative pions are tabulated in Table 4 and shown in Fig. 11. Errors indicated are due to only

†† See that the cross section of the reaction $\gamma p \rightarrow \pi^- \pi^+ p$ is largest around this energy.

††† Present model gives the cross sections $\sigma(\gamma p \rightarrow N^* \rightarrow \pi^- \Delta^{++}(1236))$ listed in Table 2 when λ is taken to be $\lambda=0$.

Table 4a. Laboratory momentum spectra
 $\theta_\pi = 20^\circ$

E_γ (MeV)	P_π (MeV/c)	$\frac{d^2\sigma}{dpd\Omega}$ (nb/sr·MeV/c)	E_γ (MeV)	P_π (MeV/c)	$\frac{d^2\sigma}{dpd\Omega}$ (nb/sr·MeV/c)	
1044	-350	-5.3 ± 11.0	944	-300	42.3 ± 8.4	
	-400	19.6 ± 7.9		-350	45.4 ± 8.5	
	-450	27.6 ± 8.5		-400	49.2 ± 4.6	
	-500	40.9 ± 6.6		-450	85.8 ± 6.1	
	-550	93.2 ± 6.5		-500	152 ± 5.4	
	-600	131.3 ± 5.0		-550	177.1 ± 4.3	
	-650	151.5 ± 3.7		-600	128.1 ± 3.0	
	-700	119.5 ± 3.1		-650	56.6 ± 2.3	
			-700	18.7 ± 2.9		
844	-150	19.0 ± 22.6	744	-150	28.1 ± 23.7	
	-200	30.7 ± 12.2		-200	58.9 ± 12.2	
	-250	63.3 ± 10.2		-250	48.3 ± 9.2	
	-300	44.5 ± 8.0		-300	122.1 ± 6.2	
	-350	85.4 ± 6.4		-350	155.3 ± 5.3	
	-400	120.3 ± 4.3		-400	128.6 ± 3.4	
	-450	180.1 ± 4.0		-450	63.3 ± 2.8	
	-500	142.2 ± 3.3		-500	17.0 ± 1.9	
	-550	57.1 ± 2.4				
	-600	15.9 ± 1.8				
	-650	6.6 ± 3.5				
-700	-0.0 ± 0.2					
1044	300	98.1 ± 28.9	944	200	20.5 ± 25.5	
	400	72.9 ± 19.8		250	41.9 ± 23.7	
	450	73.5 ± 11.9		300	104.6 ± 15.4	
	500	87.7 ± 10.6		350	95.1 ± 13.3	
	550	120.5 ± 9.3		400	117.8 ± 6.9	
	600	145.5 ± 8.2		450	124.9 ± 13.7	
	650	145 ± 5.5		500	120.9 ± 11.5	
	700	156.3 ± 6.1		550	153.4 ± 7.0	
		600	113.3 ± 6.1			
		650	67.4 ± 4.4			
		700	49.6 ± 5.2			
844	200	98.4 ± 23.5	744	150	19.6 ± 25.7	
	250	139.2 ± 22.0		200	60.5 ± 16.2	
	300	123.4 ± 14.9		250	65.0 ± 14.5	
	350	150.7 ± 10.5		300	127.1 ± 13.5	
	400	137.7 ± 8.7		350	164.6 ± 9.1	
	450	160.1 ± 12.1		400	171.8 ± 9.1	
	500	132.3 ± 10.0		450	109.2 ± 7.3	
	550	46.3 ± 5.1		500	46.0 ± 6.6	
	600	10.8 ± 5.9				
	650	21.4 ± 10.0				
700	4.8 ± 0.5					

Table 4b. Laboratory momentum spectra
 $\theta_{\pi}=40^{\circ}$

E_{γ} (MeV)	P_{π} (MeV/c)	$\frac{d^2\sigma}{dpd\Omega}$ (nb/sr·MeV/c)	E_{γ} (MeV)	P_{π} (MeV/c)	$\frac{d^2\sigma}{dpd\Omega}$ (nb/sr·MeV/c)
1044	-100	24.3±29.4	944	-100	-1.9±27.9
	-150	6.9±19.4		-150	-2.5±16.8
	-200	2.3±15.8		-200	48.4±12.3
	-250	-0.8±12.6		-250	37.7±10.6
	-300	25.6±10.2		-300	20.9± 8.5
	-350	33.6± 8.7		-350	18.4± 6.3
	-400	17.7± 7.3		-400	54.2± 6.0
	-450	42.9± 6.5		-450	86.9± 4.7
	-500	58.5± 5.3		-500	87.8± 3.4
	-525	65.9± 3.9		-525	65.3± 3.1
	-550	75.6± 3.8		-550	36.3± 2.4
	-600	41.7± 2.4		-600	11.0± 2.0
	-650	17.1± 1.7		-650	-1.6± 8.5
-700	-1.0± 3.8				
844	-100	6.3±23.3	744	-100	-8.8±18.9
	-150	23.5±14.4		-150	20.8±11.9
	-200	16.6±10.5		-200	59.0± 9.4
	-250	31.7± 9.1		-250	67.4± 6.9
	-300	39.4± 6.9		-300	78.1± 4.7
	-350	74.1± 4.7		-350	68.3± 3.5
	-400	104.8± 4.1		-400	28.7± 2.4
	-450	57.5± 2.9		-450	5.2± 1.9
	-500	13.2± 2.1		-500	4.4± 6.0
	-550	4.1± 2.9			
1044	100	8.3±42.9	944	100	-30.2±35.0
	150	33.6±28.6		150	31.6±24.5
	200	67.7±26.7		200	56.8±22.2
	250	42.6±22.9		225	41.4±19.1
	300	69.4±17.9		250	97.5±21.4
	350	69.3±16.9		300	58.8±15.2
	400	30.5±13.5		350	56.1±14.0
	425	38.8±12.3		400	72.7±10.9
	450	36.8±11.1		425	70.9±11.2
	500	79.8± 9.6		450	81.5± 9.1
	550	71.9± 8.7		500	65.3± 7.7
	600	42.0± 7.3		550	47.0± 6.9
	700	50.0±12.0		600	33.6± 6.9
844	100	12.8±27.8	744	100	16.3±23.6
	150	27.3±20.3		150	51.6±16.7
	200	28.2±18.4		200	90.1±13.7
	225	78.2±16.8		225	82.2±12.8
	250	61.5±17.7		250	93.6±14.2
	275	83.2±16.8		275	122.2±13.1
	300	83.8±12.5		300	142.7±10.0
	350	110.3±11.2		350	104.2± 8.5
	400	93.6± 8.5		400	68.9± 6.5
	425	56.2± 9.0		425	63.7± 5.9
	450	57.9± 7.0		450	21.7± 6.3
	500	19.0± 6.1		500	84.3±22.0
	550	5.3±10.4			

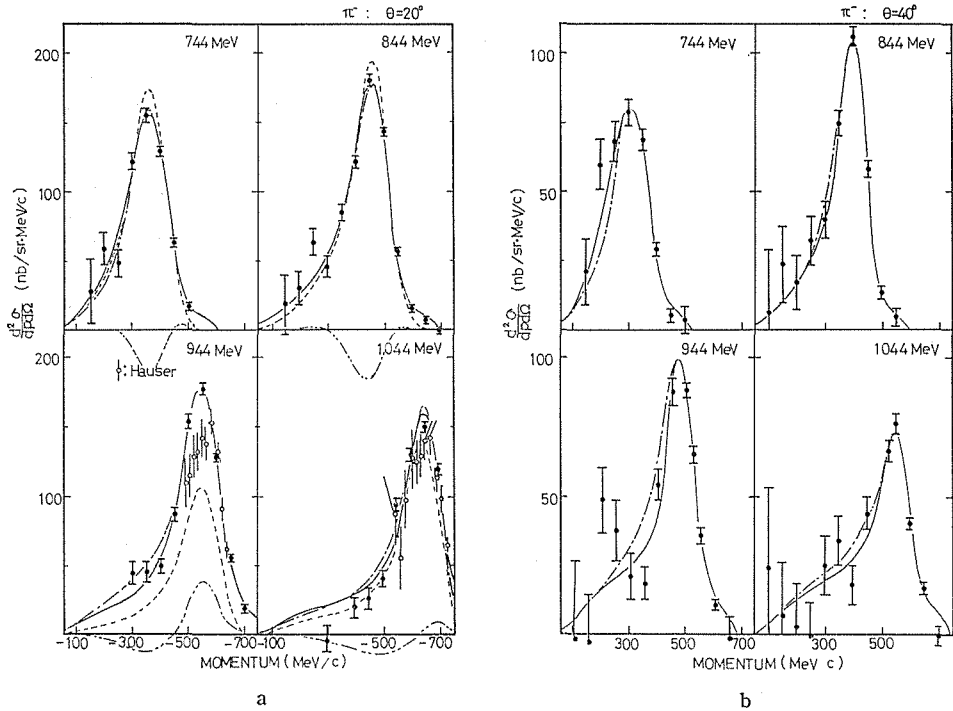
Table 4c. Laboratory momentum spectra
 $\theta_\pi = 60^\circ$

E_γ (MeV)	P_π (MeV/c)	$\frac{d^2\sigma}{dpd\Omega}$ (nb/sr·MeV/c)	E_γ (MeV)	P_π (MeV/c)	$\frac{d^2\sigma}{dpd\Omega}$ (nb/sr·MeV/c)
1044	-100	34.9±21.4	944	-100	-1.5±23.8
	-150	23.0±12.3		-150	12.8±10.1
	-200	17.3± 9.2		-200	4.6± 7.0
	-250	21.3± 7.3		-250	9.8± 5.5
	-300	27.2± 5.7		-300	21.9± 4.4
	-350	22.0± 4.4		-350	38.9± 2.5
	-400	25.6± 4.8		-375	42.8± 3.7
	-425	38.9± 4.3		-400	45.3± 3.1
	-450	37.5± 3.4		-450	14.0± 1.8
	-475	27.5± 2.8			
	-500	14.2± 2.0			
-550	4.0± 2.0				
844	-100	-10.5±19.5	744	-100	16.9±13.9
	-150	17.1±10.2		-150	45.9±10.1
	-200	36.6± 5.5		-200	49.5± 5.9
	-250	31.8± 4.9		-250	54.4± 4.8
	-300	45.9± 3.1		-300	37.5± 2.5
	-350	47.3± 2.2		-325	20.1± 2.4
	-400	16.4± 1.6		-350	10.7± 1.9
	-450	0.7± 1.7		-400	9.1± 2.6
1044	100	55.5±24.1	944	100	-36.2±19.5
	150	74.5±19.6		150	22.5±17.9
	175	108.2±19.0		175	-11.4±17.4
	200	65.0±18.0		200	50.5±15.5
	225	30.4±18.6		225	92.4±15.8
	250	62.0±15.4		250	50.1±12.3
	275	37.9±22.9		275	76.7±18.9
	300	33.9±10.3		300	58.4± 9.0
	325	51.4±16.8		350	52.4± 6.3
	350	19.9± 7.5		375	20.8± 9.9
	375	41.1±12.8		400	26.5± 5.2
	400	41.6± 7.2		425	29.3± 8.0
	425	36.5± 8.8		450	7.7± 4.6
	450	35.4± 6.0		500	14.2± 7.0
	500	7.0± 4.7			
	550	-4.1± 5.1			
425	23.4± 9.5				
844	100	27.7±21.7	744	100	-3.0±22.2
	150	12.5±18.7		150	91.6±18.1
	175	24.0±18.1		175	124.0±17.1
	200	74.9±17.1		200	92.4±17.3
	250	67.8±13.3		250	121.4±12.3
	300	57.3± 9.5		300	94.9± 8.9
	350	38.6± 6.5		350	44.6± 6.1
	400	26.7± 4.9		400	32.0± 9.4
	450	-4.0± 7.1			

Table 4d. Laboratory momentum spectra
 $\theta_{\pi}=90^{\circ}$

E_{γ} (MeV)	P_{π} (MeV/c)	$\frac{d^2\sigma}{dpd\Omega}$ (nb/sr·MeV/c)	E_{γ} (MeV)	P_{π} (MeV/c)	$\frac{d^2\sigma}{dpd\Omega}$ (nb/sr·MeV/c)
1044	150	47.4 ± 32.7	944	150	38.6 ± 27.5
	175	39.8 ± 26.2		175	29.2 ± 22.7
	200	25.2 ± 24.7		200	67.5 ± 21.3
	225	38.5 ± 18.9		225	41.1 ± 15.8
	250	19.5 ± 14.9		250	38.9 ± 12.6
	275	17.3 ± 10.5		275	48.8 ± 7.7
	300	41.7 ± 9.3		300	6.4 ± 7.4
	325	26.5 ± 9.3		325	19.6 ± 6.9
	350	14.5 ± 8.9		350	6.2 ± 7.3
	375	14.9 ± 8.2		375	11.4 ± 13.4
	400	0.9 ± 11.7	400	0.3 ± 0.6	

counting statistics. The yields and the spectra of positive and negative pions are consistent with those of the previous experiment⁷⁾ at the laboratory angle of 60° . The negative pion spectra agree well with the Caltech data³⁾ and show a peak corresponding to the reaction (1.4). A peak corresponding to the reaction (1.5) is also seen in the positive pion spectra especially at the laboratory angle of 20° and at high energies. This peak was not so clearly observed in the bubble chamber experiments⁴⁻⁶⁾; whole the yields from the reaction (1.5) are observed in our experiment, whereas only one third of the yields from the reaction (1.5) which correspond



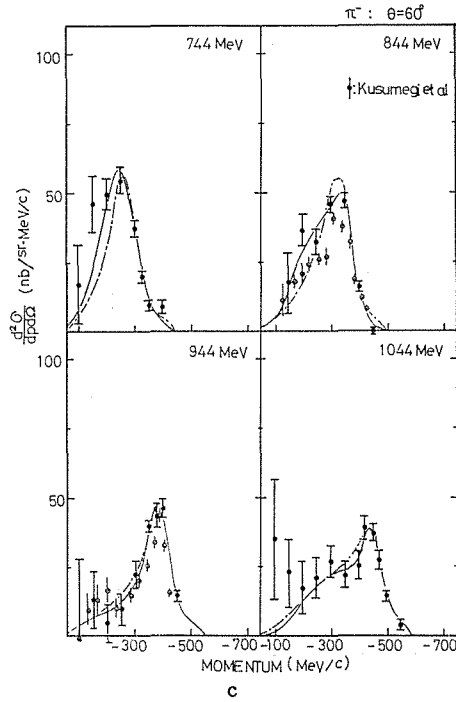
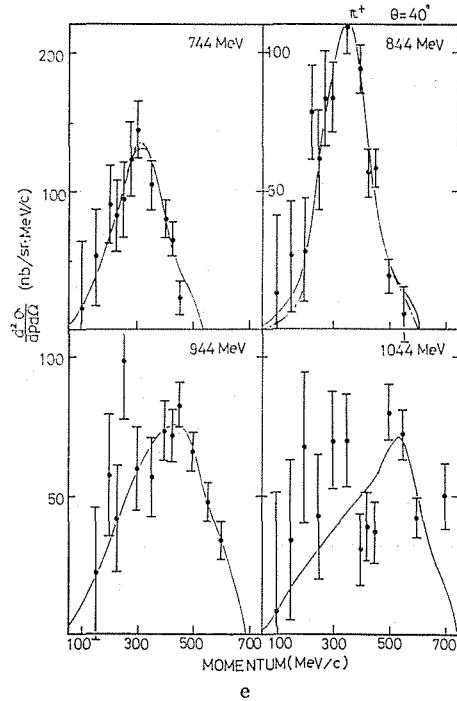
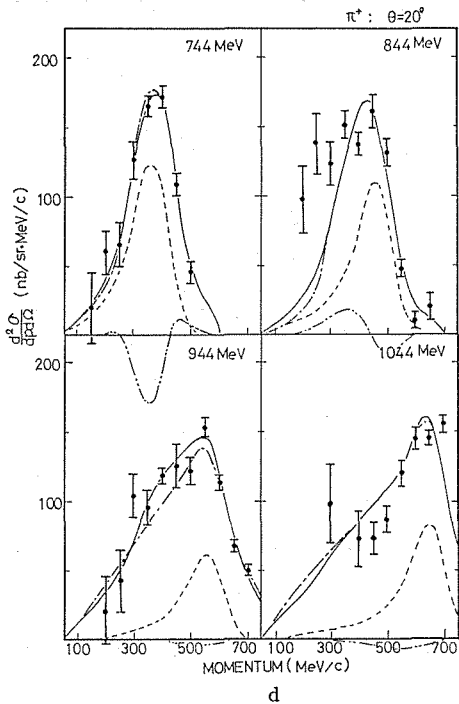


Fig. 11a—c. Laboratory momentum spectra of negative pions from the reaction $\gamma p \rightarrow \pi\pi N$. \circ —: Caltech³⁾, \circ —: Kusumegi et al²⁾, \bullet —: present. The solid curves are the calculated spectra to fit to our data by using the isospin amplitudes (see section 5 of the text). The dash-dotted curves are fitted ones by the separate fitting (see the text). The dashed and dash-two-dotted curves present the recoil pion spectra ($|A_1|^2$) and the interference terms ($2\text{Re}(A_1 \cdot A_2)$), respectively.



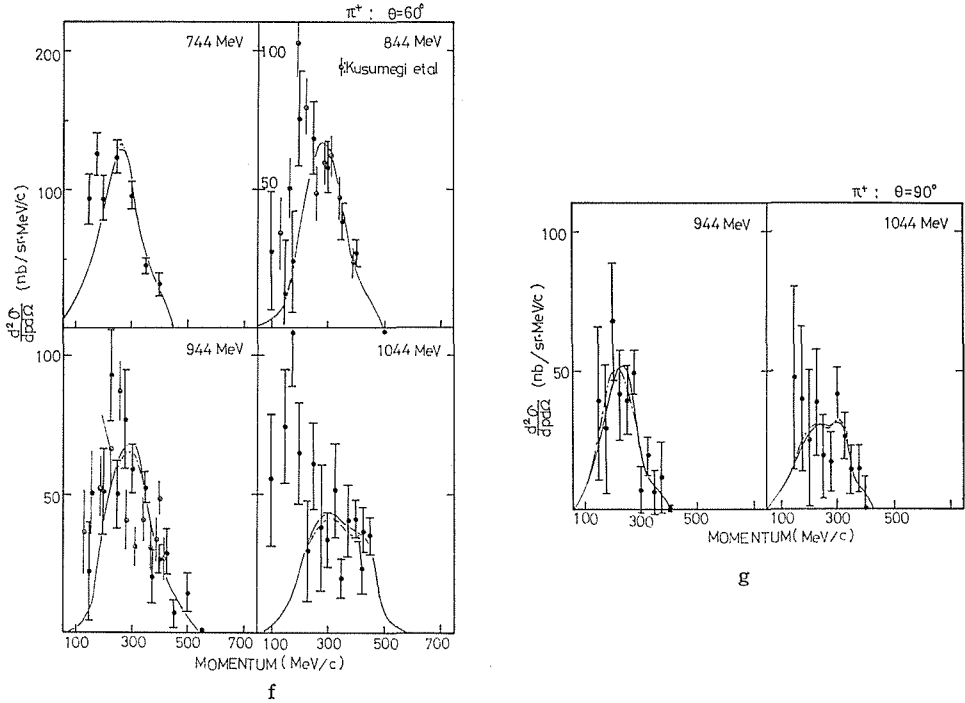


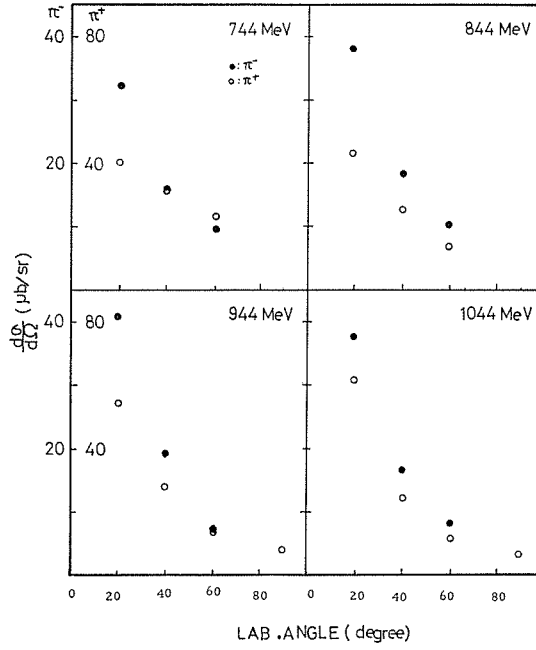
Fig. 11d—g. Laboratory momentum spectra of positive pions from the reaction $\gamma p \rightarrow \pi \pi N$. $-\odot-$: Kusumegi et al.⁷⁾, $-\bullet-$: present. The curves shown have the same meanings with those in Fig. 11a~c.

Table 5a. Result of fitting (procedure with isospin amplitudes)

E_γ (MeV)	θ^* (deg)	Lab. cross section $\frac{d\sigma}{d\Omega}$ ($\mu\text{b}/\text{sr}$)		Lab. cross section $\frac{d\sigma}{d\Omega}$ ($\mu\text{b}/\text{sr}$)		CM. cross section $\frac{d\sigma}{d\Omega^*}$ ($\mu\text{b}/\text{sr}$)		χ^2/N_f
		$\gamma p \rightarrow \pi^-$ ($\pi^+ p$)	$\gamma p \rightarrow \pi^+$ ($\pi^- p$ or $\pi^0 n$)	$\gamma p \rightarrow \pi^- \Delta^{++}$	$\gamma p \rightarrow \pi^+ \Delta^0$	$\gamma p \rightarrow \pi^- \Delta^{++}$	$\gamma p \rightarrow \pi^+ \Delta^0$	
1044	37.7	37.8 ± 0.2	62.3 ± 0.3	28.1 ± 0.8	16.9 ± 1.0	9.6 ± 0.3	5.8 ± 0.4	11.7
	69.6	17.3 ± 0.2	25.0 ± 0.3	8.8 ± 0.7	4.7 ± 0.3	4.3 ± 0.3	2.3 ± 0.3	2.1
	94.9	8.6 ± 0.2	11.6 ± 0.2	1.6 ± 0.2	2.6 ± 0.5	1.2 ± 0.1	1.9 ± 0.4	3.3
	123.5	8.1 ± 0.6	6.9 ± 0.4	2.0 ± 0.7	1.0 ± 0.3	2.8 ± 0.9	1.4 ± 0.5	0.9
944	37.0	41.1 ± 0.2	55.0 ± 0.3	20.8 ± 0.7	12.4 ± 0.5	7.4 ± 0.3	4.5 ± 0.2	2.1
	68.5	19.4 ± 0.2	27.9 ± 0.3	15.2 ± 0.8	2.4 ± 0.3	7.6 ± 0.4	1.2 ± 0.1	1.7
	93.6	7.5 ± 0.1	13.6 ± 0.3	4.1 ± 0.5	0.1 ± 0.1	3.1 ± 0.4	0.1 ± 0.1	1.9
	122.3	3.6 ± 0.1	8.0 ± 0.4	0.4 ± 0.3	0.8 ± 0.4	0.6 ± 0.4	1.1 ± 0.6	1.5
844	36.5	38.2 ± 0.2	42.5 ± 0.4	36.9 ± 0.5	20.4 ± 1.5	13.8 ± 0.2	7.6 ± 0.5	11.5
	67.6	17.9 ± 0.2	24.7 ± 0.4	17.2 ± 0.5	6.9 ± 0.8	8.7 ± 0.2	3.5 ± 0.4	0.8
	92.5	10.1 ± 0.2	12.6 ± 0.3	11.4 ± 0.6	0.4 ± 0.1	8.4 ± 0.5	0.3 ± 0.1	2.2
744	36.7	32.4 ± 0.2	40.3 ± 0.4	31.4 ± 0.9	22.0 ± 1.0	12.2 ± 0.3	8.5 ± 0.4	1.8
	67.6	16.2 ± 0.2	30.9 ± 0.3	18.7 ± 0.9	16.0 ± 0.6	9.7 ± 0.5	8.3 ± 0.3	2.5
	92.1	9.6 ± 0.2	23.5 ± 0.3	9.2 ± 0.7	13.7 ± 0.7	6.8 ± 0.5	10.1 ± 0.5	4.0

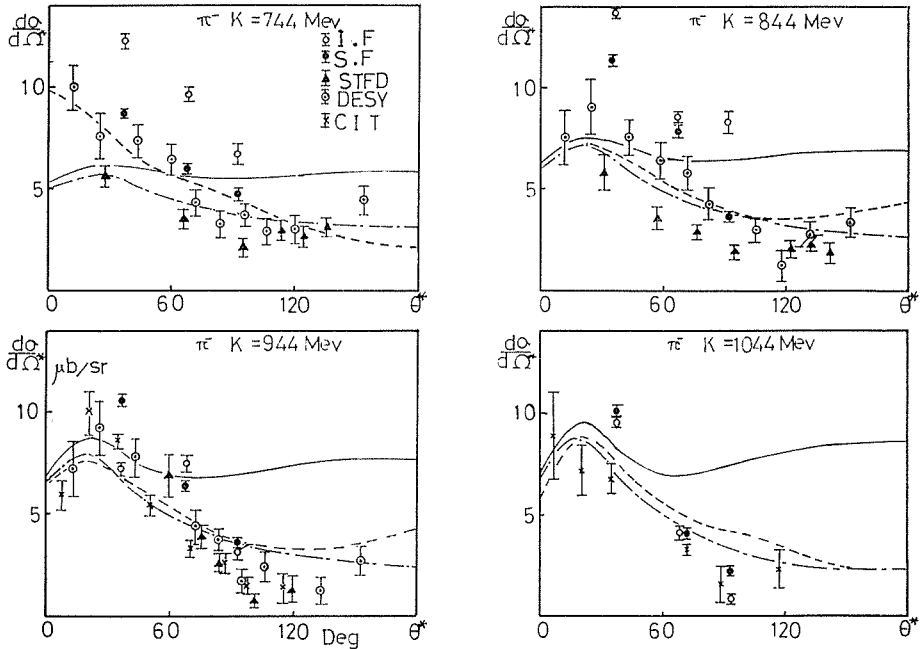
to the reaction (1.5') are observed in the bubble chamber experiments because of the decay of $\Delta^0(1236)$.

The solid curves in Fig. 11 show the calculated spectra by the method of sec-

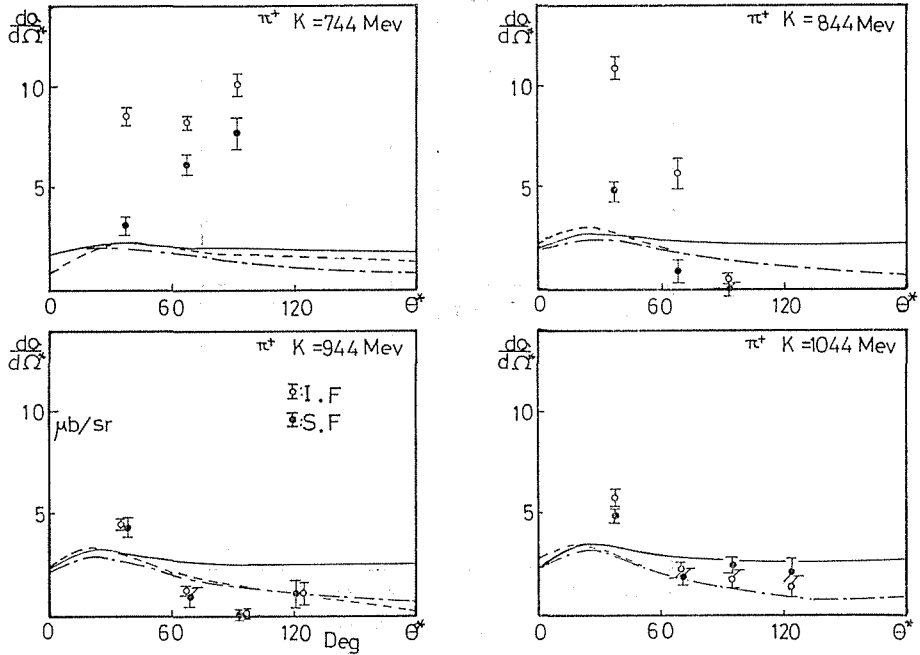


a

Fig. 12a. Laboratory differential cross sections $d\sigma/d\Omega(\gamma p \rightarrow \pi\pi N)$ obtained by integrating eq. (5.1) of the text with the obtained parameters. ●: for the reaction $\gamma p \rightarrow \pi^-(\pi^+ p)$, ○: for the reaction $\gamma p \rightarrow \pi^+(\pi N)$.



b



c

Fig. 12b,c. Centre of mass cross sections $d\sigma/d\Omega^*$ of the reaction (b) $\gamma p \rightarrow \pi^- \Delta^{++}(1236)$ and (c) $\gamma p \rightarrow \pi^- \Delta^0(1236)$. \leftarrow : Stanford²⁾, \circ : DESY²⁾, \times : Caltech³⁾, \square : present data by the fitting procedure with isospin amplitudes, \bullet : present data by the separate fitting. The curves are calculated by the gauge invariant OPE model. Solid curve: without form factor, dash-dotted curve: with form factor, dashed curve: with the phenomenological amplitudes given in section 6 of the text and with form factor at the $\pi N \Delta$ and $\pi N^* \Delta$ vertices. The form factor used is given by $e^{\lambda(t-\mu^2)}$, t : momentum transfer squared, μ : pion mass, λ : a parameter and $\lambda=0.8$ (GeV/c)⁻².

tion 5 with the obtained parameters. The curves reproduce well the observed ones.

The obtained centre of mass cross sections $d\sigma/d\Omega^*(\gamma p \rightarrow \pi^- \Delta^{++}(1236))$ are listed in Table 5 and shown in Fig. 12 together with the existing data. The obtained values of $d\sigma/d\Omega^*(\gamma p \rightarrow \pi^- \Delta^{++}(1236))$ are consistent with the results of other experiments at the energies of 944 and 1044 MeV. At the energies of 744 and 844 MeV, our cross sections have larger values than those of other experiments. At these energies, the momentum distribution of recoil pions ($\pi^- \Delta^{++}$) is considerably overlapped by the one of decay pions ($\Delta^0 \rightarrow \pi^- p$). Thus the interference between the recoil and decay pions plays a important role at these energies. Furthermore, the amplitudes are determined by using not only the negative pion spectra but also the positive pion ones, in which the large contribution due to the decay π^+ from $\Delta^{++}(1236)$ is included. In the fitting procedure, the interference of recoil and decay π^+ is also taken into account for the final state of $(\pi^+ \pi^0 n)$ which is observed in our experiment. Moreover, for the sake of the overlapping of recoil pion, decay pion and the phase space pion in the momentum spectra, some ambiguities arise in the fitting procedure even if the interference effect is ignored. These situations are clarified by using the different fitting method. In this fitting, the amplitudes

Table 5b. Result of additional fitting procedure (separate fitting)

E_γ (MeV)	θ^* (deg)	Lab. cross section $\frac{d\sigma}{d\Omega}$ ($\mu\text{b}/\text{sr}$)		Lab. cross section $\frac{d\rho}{d\Omega}$ ($\mu\text{b}/\text{sr}$)		CM. cross section $\frac{d\sigma}{d\Omega^*}$ ($\mu\text{b}/\text{sr}$)		χ^2/N_f
		$\gamma p \rightarrow \pi^-$ ($\pi^+ p$)	$\gamma p \rightarrow \pi^+$ ($\pi^- p$ or $\pi^0 n$)	$\gamma p \rightarrow \pi^- \Delta^{++}$	$\gamma p \rightarrow \pi^+ \Delta^0$	$\gamma p \rightarrow \pi^- \Delta^{++}$	$\gamma p \rightarrow \pi^+ \Delta^0$	
1044	37.3	37.3 ± 0.2	63.7 ± 0.3	31.8 ± 0.5	14.2 ± 0.5	10.9 ± 0.2	4.9 ± 0.3	π^- 14.5 π^+ 9.7
	69.6	18.4 ± 0.1	25.0 ± 0.3	8.7 ± 0.4	4.3 ± 1.1	4.2 ± 0.2	2.0 ± 0.5	π^- 1.7 π^+ 2.6
	94.9	9.1 ± 0.2	11.6 ± 0.2	3.3 ± 0.3	2.8 ± 0.6	2.5 ± 0.2	2.1 ± 0.4	π^- 1.2 π^+ 4.3
	123.5		6.8 ± 0.4		1.6 ± 0.7		2.2 ± 0.8	π^- π^+ 0.6
944	37.0	43.5 ± 0.1	54.9 ± 0.3	29.5 ± 0.5	11.6 ± 1.0	10.6 ± 0.2	4.2 ± 0.4	π^- 5.3 π^+ 1.4
	68.5	21.8 ± 0.1	27.8 ± 0.4	13.1 ± 0.5	1.9 ± 1.1	6.5 ± 0.2	0.9 ± 0.5	π^- 4.6 π^+ 1.0
	93.6	7.9 ± 0.1	13.4 ± 0.2	5.0 ± 0.3	0.0 ± 0.4	3.7 ± 0.2	0.0 ± 0.3	π^- 0.8 π^+ 2.3
	122.3		8.2 ± 0.3		0.8 ± 0.7		1.1 ± 0.8	π^- π^+ 1.5
844	36.5	38.2 ± 0.1	40.4 ± 0.4	30.1 ± 0.5	13.1 ± 1.3	11.3 ± 0.2	4.9 ± 0.5	π^- 2.4 π^+ 15.0
	67.6	18.3 ± 0.1	23.2 ± 0.3	15.3 ± 0.5	1.8 ± 1.0	7.8 ± 0.3	0.9 ± 0.5	π^- 0.6 π^+ 1.3
	92.5	9.1 ± 0.1	12.5 ± 0.3	5.4 ± 0.3	0.0 ± 0.5	4.0 ± 0.2	0.0 ± 0.4	π^- 4.9 π^+ 2.1
744	36.7	30.9 ± 0.2	40.1 ± 0.4	22.5 ± 0.6	8.1 ± 1.2	8.7 ± 0.2	3.1 ± 0.5	π^- 3.1 π^+ 1.2
	67.6	15.2 ± 0.1	30.7 ± 0.3	11.8 ± 0.5	12.1 ± 1.0	6.1 ± 0.3	6.2 ± 0.5	π^- 3.6 π^+ 3.1
	92.1	8.5 ± 0.1	23.5 ± 0.3	6.2 ± 0.4	10.5 ± 1.2	4.6 ± 0.3	7.7 ± 0.8	π^- 4.3 π^+ 4.3

Table 6. Result of fitting procedure: s -channel isospin amplitudes

k MeV	θ_1^* deg	$T_1(\theta_1^*)^R$ ($\mu\text{b}/\text{sr}$) ^{1/2}	$T_1(\theta_1^*)^I$ ($\mu\text{b}/\text{sr}$) ^{1/2}	$T_3(\theta_1^*)$ ($\mu\text{b}/\text{sr}$) ^{1/2}
1044	37.7	4.3 ± 0.04	4.3 ± 0.04	1.1 ± 0.1
	69.6	-1.8 ± 0.2	2.6 ± 0.1	0.5 ± 0.2
	94.9	-1.2 ± 0.2	1.5 ± 0.1	1.1 ± 0.2
	123.5	-2.4 ± 0.2	-0.9 ± 0.7	0.2 ± 0.2
944	37.0	0.1 ± 0.06	3.1 ± 0.1	2.4 ± 0.1
	68.5	1.7 ± 0.1	0.4 ± 0.6	2.4 ± 0.1
	93.6	1.7 ± 0.1	0.6 ± 0.4	0.8 ± 0.1
	122.3	-1.4 ± 0.4	0.7 ± 0.2	0.6 ± 0.1
844	36.5	-1.5 ± 0.3	5.3 ± 0.04	1.5 ± 0.2
	67.6	-0.6 ± 0.3	4.2 ± 0.1	0.7 ± 0.3
	92.5	3.1 ± 0.1	0.3 ± 0.3	1.2 ± 0.1
744	36.7	-0.6 ± 0.1	4.6 ± 0.1	2.8 ± 0.1
	67.6	0.5 ± 0.07	1.0 ± 0.3	4.2 ± 0.1
	92.1	-0.6 ± 0.1	2.4 ± 0.1	3.8 ± 0.1

a_1^+ and a_2^+ are not decomposed into isospin amplitudes; namely, by ignoring all the interference terms in the eq.(5.1), the positive and negative pion spectra are fitted separately. This fitting is called the separate fitting. The obtained cross sections $d\sigma/d\Omega^*(\gamma p \rightarrow \pi^- \Delta^{++}(1236))$ by two different methods agree with each other at the energies of 944 and 1044 MeV. At these energies, the separation of recoil

pions from decay and phase space ones is good. Furthermore, at the energies of 744 and 844 MeV, results by the separate fitting agree well with the ones of bubble chamber experiment⁴⁾. Two different fitting showed nearly the same confidence level of χ^2 -value.

The result of fitting procedure with isospin amplitudes gives us some informations on the s-channel isospin amplitudes of the reaction (1.3). The present procedure shows that the amplitude $T_1(\theta_1)$ has a certain amount of imaginary part (see Table 6) and suggests the existence of s-channel resonances which decay into $\pi\Delta(1236)$.

In the present experiment, cross sections $d\sigma/d\Omega^*(\gamma p \rightarrow \pi^+\Delta^0(1236))$ are also deduced and shown in Fig. 12c. These cross sections have similar angular behaviours as those of $d\sigma/d\Omega^*(\gamma p \rightarrow \pi^-\Delta^{++}(1236))$ except at the energy of 744 MeV. The values of $d\sigma/d\Omega^*(\gamma p \rightarrow \pi^+\Delta^0(1236))$ are not so small as shown by the results of bubble chamber experiments⁴⁻⁶⁾ in the present energy region.

The obtained ratios r_1 are illustrated in Fig. 13. The mean values of r_1 at each energy are calculated by taking into account of statistical weight and found to be in the range of 0.1 to 0.8 depending on the energy. On the contrary, the values of r_2 at DESY⁴⁾ indicate that the ratio r_1 is much smaller than 0.1 in our energy region.

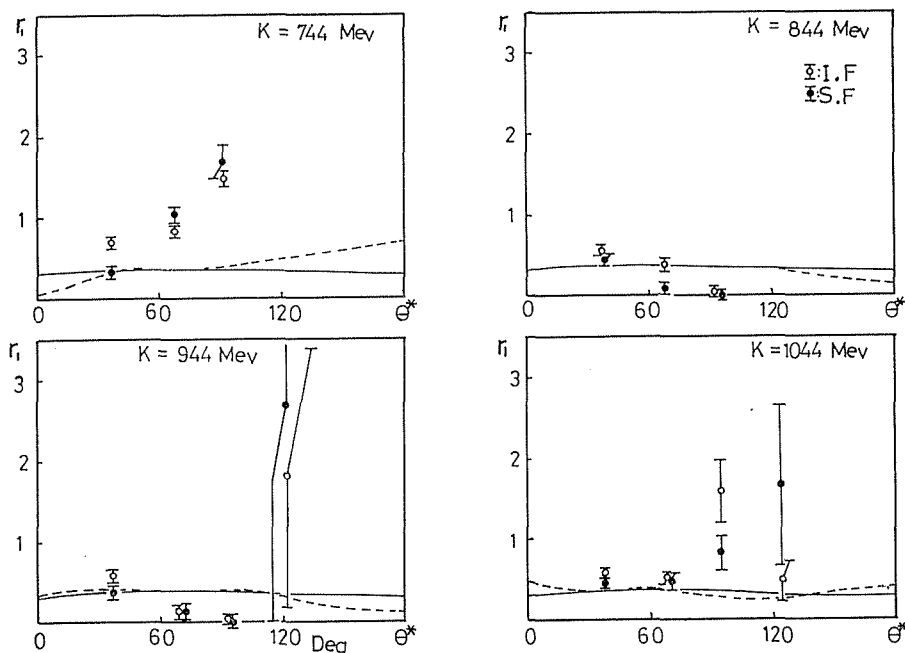


Fig. 13. The ratio of cross sections (see the text). $|\circ|$: fitting with isospin amplitudes, $|\bullet|$: separate fitting. Solid and dashed curves have the same meanings with those in Fig. 12.

7-2. Comparison with the theoretical calculations

The solid curves in Fig. 12 present the calculated cross sections by the gauge invariant one pion exchange model⁹⁾ (G.I.OPE model). The dash-dotted curves show the calculated cross sections by the G.I.OPE model with the form factor given

in section 6. The dashed curves give the calculated ones by the gauge invariant one pion exchange model with the phenomenological amplitudes described in section 6 and with the form factor (present model). The calculated cross sections $d\sigma/d\Omega^*(\gamma p \rightarrow \pi^- \Delta^{++}(1236))$ by the present model explain our experimental results qualitatively. The agreement for the present model is better than the ones for the G.I.OPE model with and without the form factor. At the energy of 744 MeV, the calculated cross sections $d\sigma/d\Omega^*(\gamma p \rightarrow \pi^- \Delta^{++}(1236))$ by the present model agree well with the ones obtained by the separate fitting. The large difference between the calculated cross sections by the G.I.OPE model and by the present model at the energy of 744 MeV is due to the resonance amplitude of $D_{13}(1525)$ which is taken into account in the present model.

The present model gives about 75 % of the value listed in Table 2 for the cross section $\sigma(\gamma p \rightarrow D_{13}(1525) \rightarrow \pi^- \Delta^{++}(1236))$ because of the form factor. The present model also gives nearly flat cross sections for the reaction (1.3) below 1.1 GeV when the form factor is ignored. Thus the form factor plays an important role in the present model.

The observed cross sections $d\sigma/d\Omega^*(\gamma p \rightarrow \pi^+ \Delta^0(1236))$ are explained qualitatively by the present model at the energies of 944 and 1044 MeV. But the agreement is poor at the energies of 744 and 844 MeV.

The calculated ratios r_1 by the present model and by the G.I.OPE model are shown in Fig. 13. At the energy of 744 MeV, the obtained ratio r_1 by both fitting procedures are larger than the theoretical calculations. These differences may be due to the systematic error of the fitting procedure which was mentioned above.

The results of fitting procedure of observed spectra with isospin amplitudes show that the amplitude $T_3(\theta_1)$ has the values nearly equal to those of the real part of $T_1(\theta_1)$ in our energy region (see Table 6). The ratio of amplitudes $|T^3|/|Re(T^1)|$ is $1 \sim 2$ for the present model when the parameters listed in Table 3 are used. In G.I.OPE model, the ratio $|T^3|/|Re(T^1)| = |B^3|/|B^1|$ is about $\sqrt{5}$ below 1 GeV; see eq. (6.2), where H^I and H^{III} contribute mainly below 1 GeV¹⁾.

As mentioned above, there are some discrepancies between our experimental results and the theoretical ones. In order to clarify these discrepancies, more experimental and theoretical investigations on the reactions (1.1) and (1.3) are required. The G.I.OPE model gives small cross sections for the reaction $\gamma + p \rightarrow \pi^0 + \Delta^+(1236)$ below 1 GeV (about 1/100 of the cross section of the reaction (1.4)) owing to the followings; only the amplitude H^{IV} contributes to the reaction $\gamma + p \rightarrow \pi^0 + \Delta^+(1236)$ and is much smaller than the amplitudes H^I and H^{III} in these energies¹⁾; whereas H^I and H^{III} contribute mainly to the reaction (1.4). Thus the investigations on the reaction $\gamma + p \rightarrow \pi^0 + \Delta^+(1236)$ will give valuable informations on the contributions of s-channel resonances and on other diagrams to the reaction (1.3).

For the isospin analysis of the reaction $\gamma + N \rightarrow \pi + \Delta(1236)$, experiments on the reaction $\gamma + n \rightarrow \pi + \Delta(1236)$ are desired.

The phenomenological amplitudes will be determined more precisely when the data on the decay density matrices⁴⁾ are taken into account.

Acknowledgement

The author would like to express his sincere thanks to Dr. M. Mishina for the

guidance throughout this work. He is deeply grateful to Prof. S. Fukui and Dr. K. Ukai for their continuous encouragement in this work.

The author is particularly indebted to Mr. K. Ueno for his partnership in every stage of this work.

Thanks are also due to Prof. A. Kusumegi, Prof. Y. Murata, Dr. K. Takamatsu, Dr. S. Iwata, Dr. I. Sato, Dr. T. Miyachi, Mr. Y. Inagaki and Mr. T. Ohsuka for the collaboration in the early stage of this work.

He is indebted to Prof. K. Miyake and Prof. T. Nakamura for their valuable discussions.

The author thanks to Prof. S. Yamaguchi and the members of synchrotron operation crew of the Institute for Nuclear study for their operating efforts.

The numerical calculations were done on the computers FACOM 230-60 at Nagoya University Computer centre Nagoya University and TOSBAC 3400 at Institute for Nuclear Study University of Tokyo.

Appendix

Helicity amplitudes for $\gamma p \rightarrow \pi \Delta$ through s-channel resonances

In this appendix the helicity amplitudes for the reaction

$$\gamma + p \rightarrow N^* \rightarrow \pi + \Delta \quad (\text{A.1})$$

are presented.

(1) Formalism

The particles in the initial and final states of the reaction (A.1) are called particle 1, 2, 3 and 4 corresponding to the photon, proton, pion and Δ , respectively. The three momentum of the i-th particle is presented by P_i in the centre of mass system. We choose the z- and y-axes along the direction of P_1 and $P_1 \times P_3$, respectively, in the cms. If we quantize the initial and final spins along the direction of P_1 and P_3 , the helicities of the initial and final states are given as follows,

$$\lambda = \lambda_1 - \lambda_2 \quad (\text{A.2})$$

$$\mu = \lambda_3 - \lambda_4 \quad (\text{A.3})$$

where λ_i denotes the helicity of the i-th particle. The total helicity amplitude for the reaction (A.1) is given by the formula^{21,22)},

$$R_{\mu\lambda}(\theta) = \frac{1}{4\pi} \sum_J (2J+1) \langle JM \lambda_3 \lambda_4 | R(J) | JM \lambda_1 \lambda_2 \rangle d_{\lambda\mu}^J(\theta), \quad (\text{A.4})$$

where J and M denote the total and third component of angular momentum, respectively. Therefore, J represent the spin of the s-channel resonance N^* in the eq.(A.1). For the amplitude $\langle JM \lambda_3 \lambda_4 | R(J) | JM \lambda_1 \lambda_2 \rangle$, the following expansion is presented^{21,22)},

$$\langle JM \lambda_3 \lambda_4 | R(J) | JM \lambda_1 \lambda_2 \rangle = \sum_{S' L' J' \epsilon} \langle JM \lambda_3 \lambda_4 | J M L' S' \rangle \cdot \langle J M L' S' | R(J) |$$

$$\begin{aligned}
& |JM J' \varepsilon \frac{1}{2}\rangle \cdot \langle JM J' \varepsilon \frac{1}{2} | JM \lambda_1 \lambda_2 \rangle \\
&= \sum_{J' \varepsilon} C_{L' J' \varepsilon}^{J \mu \lambda} \cdot \langle JML' \frac{3}{2} | R(J) | JM J' \varepsilon \frac{1}{2} \rangle, \tag{A.5}
\end{aligned}$$

where J' denotes the total angular momentum of photon, ε ($\varepsilon=0$ or 1) characterizes the type of photon, namely, $\varepsilon=0$ corresponds to the magnetic radiation, and $\varepsilon=1$ corresponds to the electric radiation. L' is the orbital angular momentum of particle 3, S' denotes the total spin of the final state and has the value of $\frac{3}{2}$ in the present reaction. The coefficient $C_{L' J' \varepsilon}^{J \mu \lambda}$ is given as,

$$C_{L' J' \varepsilon}^{J \mu \lambda} = \langle JM \lambda_3 \lambda_3 | JML' \frac{3}{2} \rangle \cdot \langle JM J' \frac{1}{2} | JM \lambda_1 \lambda_2 \rangle. \tag{A.6}$$

The left side of eq.(A.5) corresponds to the transition amplitude with the definite J but a mixed parity. The parity of the initial state is given by the parity of electro-magnetic multipole radiation²³⁾. The positive and negative parity states of the final state are given:

$$\frac{1}{\sqrt{2}} \{ |JM \lambda_3 \lambda_4 \rangle + (-1)^{J+3/2} |JM \lambda_3 \lambda_4 \rangle \}, \tag{A.7}$$

$$\frac{1}{\sqrt{2}} \{ |JM \lambda_3 \lambda_4 \rangle + (-1)^{J+1/2} |JM \lambda_3 \lambda_4 \rangle \}. \tag{A.8}$$

Thus we can assign the amplitude $\langle JML' \frac{3}{2} | R(J) | JM J' \varepsilon \frac{1}{2} \rangle$ to the each resonance with the definite spin and parity according to the conservation law of angular momentum and parity. In the preceding formulae, the helicity of particle 3 (pion) is zero,

$$\lambda_3 = 0. \tag{A.9}$$

There are sixteen combinations of initial and final states helicities. The transition amplitudes $T_{\mu\lambda}$ of the reaction $\gamma N \rightarrow \pi d$ is connected to $T_{-\mu-\lambda}$ by the conservation law of parity²¹⁾,

$$T_{\mu\lambda}(\theta) = (-1)^{\mu-\lambda} T_{-\mu-\lambda}(\theta). \tag{A.10}$$

Then the number of independent combination of helicities is reduced to eight. We can restrict the values of λ and μ as follows,

$$\lambda = \frac{3}{2}, -\frac{1}{2}, \tag{A.11}$$

$$\mu = \frac{3}{2}, \frac{1}{2}, -\frac{1}{2}, -\frac{3}{2}, \tag{A.12}$$

where the helicity of proton (λ_2) is fixed to $-\frac{1}{2}$.

The above mentioned formalism is used to define the helicity amplitudes $R_{\mu\lambda}^1$ and $R_{\mu\lambda}^3$ which correspond to the reaction (A.1) with the s-channel isospin of $\frac{1}{2}$ and $\frac{3}{2}$, respectively.

(2) Cross section formula

The amplitudes $T_{\mu\lambda}^{++}$, $T_{\mu\lambda}^+$ and $T_{\mu\lambda}^0$ corresponding to the reactions $\gamma p \rightarrow \pi^- \Delta^{++}$, $\gamma p \rightarrow \pi^0 \Delta^+$ and $\gamma p \rightarrow \pi^+ \Delta^0$ are obtained by using the amplitudes $R_{\mu\lambda}^1$ and $R_{\mu\lambda}^3$ according to the manner mentioned in section 6 of the text. The cross section for the reaction $\gamma p \rightarrow \pi \Delta$ is given,

$$\frac{d\sigma}{d\Omega} = \frac{\alpha}{8\pi} \cdot G^2 \frac{m}{s} \frac{m'}{k} \cdot \sum_{\lambda=3/2, -1/2} \sum_{\mu=-3/2}^{3/2} |T_{\mu\lambda}|^2 \quad (\text{A.13})$$

where

$$\begin{aligned} \alpha &= \text{fine structure constant,} \\ G &= \pi N \Delta \text{ coupling constant, } G=15.4, \\ m, m' &= \text{mass of nucleon and } \Delta, \text{ respectively,} \\ s &= \text{total cms energy squared,} \\ k, q &= \text{magnitude of momentum } P_1 \text{ and } P_3, \text{ respectively.} \end{aligned}$$

The amplitude $T_{\mu\lambda}$ in eq.(A.13) denotes $T_{\mu\lambda}^{++}$, $T_{\mu\lambda}^+$ or $T_{\mu\lambda}^0$.

(3) Assignment of amplitudes for resonances

In this section we introduce the amplitude "F" which corresponds to the amplitude $\langle JML' \frac{3}{2} | R(J) | JM J' \epsilon \frac{1}{2} \rangle$ with the definite spin and parity. The amplitude F is written:

$$F_{2I, 2J}^{p\epsilon} = F_{i,j}^{p\epsilon} \quad (\text{A.14})$$

where p , I and J denote parity, isospin and spin of the resonance, respectively.

The amplitude $F_{i,j}^{p\epsilon}$ is described by $E_{i,j}^p$ or $M_{i,j}^p$ according to the electric ($\epsilon=1$) or magnetic ($\epsilon=0$) transition. For the resonances which are allowed to have two values of L' , we introduce the decay fractions of the resonance $N^*(J^p)$ into lower and higher values of L' ,

$$|\alpha_{i,j}^p|^2 \text{ and } |\beta_{i,j}^p|^2,$$

respectively, with condition

$$|\alpha_{i,j}^p|^2 + |\beta_{i,j}^p|^2 = 1. \quad (\text{A.15})$$

Using $E_{i,j}^p$, $M_{i,j}^p$, $\alpha_{i,j}^p$ and $\beta_{i,j}^p$, we can describe the amplitude F in terms of

$$\alpha_{i,j}^p \cdot E_{i,j}^p, \beta_{i,j}^p \cdot E_{i,j}^p, \alpha_{i,j}^p \cdot M_{i,j}^p \text{ or } \beta_{i,j}^p \cdot M_{i,j}^p.$$

Examples are listed in Table 3 for some resonances.

(4) Energy dependence of the amplitudes

The energy dependence of the amplitude F is presented by the formula,

$$F(W) = F(W_0) \cdot \left(\frac{k_0 q_0}{k q} \right)^{1/2} \cdot \frac{W \cdot (\Gamma \cdot \Gamma_\gamma)^{1/2}}{s_0 - s - i \cdot W \cdot \Gamma} \quad (\text{A.16})$$

with

$$\Gamma = \Gamma_0 \cdot \left(\frac{q}{q_0} \right)^{2L'+1} \cdot \left(\frac{q_0^2 + X^2}{q^2 + X^2} \right)^{L'} \quad (\text{A.17})$$

$$\Gamma_\gamma = \Gamma_0 \cdot \left(\frac{k}{k_0} \right)^{2J'} \cdot \left(\frac{k_0^2 + X^2}{k^2 + X^2} \right)^{J'} \quad (\text{A.18})$$

where

$W = \sqrt{s}$, total cms energy,

Γ = total width of resonance,

W_0, Γ_0, k_0 and q_0 = values of W, Γ, k and q at the resonance energy, respectively.

X^2 = parameter discussed by Jackson¹⁶).

The values of W_0, Γ_0 and X^2 given by Walker¹⁷) are used for the numerical calculation.

We can introduce a constant phase factor to the amplitude of each resonance multiplying to $F(W)$:

$$F(W) \cdot e^{i\phi}. \quad (\text{A.19})$$

(5) Conditions on the amplitudes for some resonances

Investigations on the single pion photoproduction show that the resonances $D_{13}(1525)$ and $F_{15}(1688)$ are scarcely photoexcited through the initial states with helicity $\pm \frac{1}{2}$. We assume here after that these conditions stand strictly for the resonances $D_{13}(1525), F_{15}(1688)$ and $D_{15}(1670)$. Then following equations are given,

$$D_{13}(1525): C_{L_1^{(3)}\mu}^{(2/3)\mu-(1/2)1} \cdot E_{12}^- + C_{L_2^{(3/2)}\mu}^{(3/2)\mu-(1/2)0} \cdot M_{13}^- = 0 \quad (\text{A.20})$$

$$F_{15}(1688): C_{L_2^{(5/2)}\mu}^{(5/2)\mu-(1/2)1} \cdot E_{15}^+ + C_{L_3^{(5/2)}\mu}^{(5/2)\mu-(1/2)0} \cdot M_{15}^+ = 0 \quad (\text{A.21})$$

$$D_{15}(1670): C_{L_2^{(5/2)}\mu}^{(5/2)\mu-(1/2)0} \cdot M_{15}^- + C_{L_3^{(5/2)}\mu}^{(5/2)\mu-(1/2)1} \cdot E_{15}^- = 0 \quad (\text{A.22})$$

Due to the conservation law of parity (see eq.(A.10~12)) and the above conditions, the initial helicity is restricted to only one value $\left(\lambda = \frac{3}{2} \right)$ for the resonances $D_{13}(1525)$ $F_{15}(1688)$ and $D_{15}(1670)$. The initial helicity for the resonances $P_{11}(1460)$ and $S_{11}(1550)$ is restricted to one value $\left(\lambda = -\frac{1}{2} \right)$ because the spin of these two resonances is $\frac{1}{2}$. We give the following expression to the coefficient $C_{L_1^{(\mu)}\lambda}^{J_1^{(\mu)}\lambda}$ for all the above resonances using the Clebsch-Gordan coefficients,

$$C_{L_1^{(\mu)}\lambda}^{J_1^{(\mu)}\lambda} = \sqrt{\frac{(2L'+1)(2J'+1)}{(2J+1)^2}} \cdot \langle J\mu | L' \frac{3}{2}; 0\mu \rangle \langle JM | J' \frac{1}{2}; \lambda_1 - \lambda_2 \rangle, \quad (\text{A.23})$$

with

$$M = \lambda = \lambda_1 - \lambda_2. \quad (\text{A.24})$$

Then the eqs.(A.20~22) are reduced to the followings,

$$D_{13}(1525): E_{13}^-/M_{13}^- = \sqrt{3} \quad (\text{A.25})$$

$$F_{15}(1688): E_{15}^+/M_{15}^+ = \sqrt{2} \quad (\text{A.26})$$

$$D_{15}(1670): M_{15}^-/E_{15}^- = \sqrt{2}. \quad (\text{A.27})$$

(6) Order of amplitudes

If only the reaction (A.1) through resonances with $I = \frac{1}{2}$ is taken into account in the reaction $\gamma p \rightarrow \pi^- \Delta^{++}$, the cross section is presented by the equation,

$$\frac{d\sigma}{d\Omega} = \frac{\alpha G^2}{2(4\pi)^3} \cdot \frac{m}{s} \frac{m'}{k} \frac{q}{2} \cdot \sum_{\lambda=3/2, -1/2} \sum_{\mu=-3/2}^{3/2} \left| \sum_J [(2J+1) \cdot \sum_{L'J'} C_{L'J'}^{I\mu\lambda e} \cdot F_{1,2J}^p \cdot d_{\lambda\mu}^J(\theta)] \right|^2. \quad (\text{A.28})$$

The total cross section for the reaction $\gamma p \rightarrow N^*_{\frac{1}{2}} \rightarrow \pi^- \Delta^{++}$ through the resonance with $I = \frac{1}{2}$ and with the definite spin and parity is obtained by integrating eq. (A.28) over the angle θ ,

$$\sigma(N^*_{\frac{1}{2}}(J^p)) = \frac{(2J+1)}{4(4\pi)^2} \cdot \alpha G^2 \cdot \frac{m \cdot m'}{s} \frac{q}{k} \cdot \sum_{\lambda=3/2, -1/2} \sum_{\mu=-3/2}^{3/2} \left| \sum_{L'J'} C_{L'J'}^{I\mu\lambda e} \cdot F_{1,2J}^{pe} \right|^2. \quad (\text{A.29})$$

We can estimate the order of amplitudes $F_{1,2J}^{pe}$ for some resonances using eq. (A.29) and the values of cross sections for the reaction $\gamma p \rightarrow \pi^- \Delta^{++}$ given in Table 2. The estimated values are listed in Table 3. In those calculations, conditions on the amplitudes $F_{1,2J}^p$ presented in the preceding section are used. For each resonance which is allowed to have two values of L' , only the lower value of L' is taken into account in those calculations.

REFERENCES

- 1) D. Lüke and P. Söding, in Springer Tract in Modern Physics, ed. G. Hähler, vol. 59 (Springer-Verlag, Berlin Heidelberg New York, 1971) p. 39.
- 2) J. V. Allaby, H. L. Lynch and D. M. Ritson, Phys. Rev. **142** (1966) 887.
- 3) M. G. Hauser, Phys. Rev. **160** (1967) 1215.
- 4) ABBHHM-collabration, Phys. Rev. **175** (1968) 1669.
- 5) Cambridge Bubble Chamber Group, Phys. Rev. **163** (1967) 1510.
- 6) G. Gialanella, A. Piazza, G. Susino, L. Fiore and G. C. Mantovani, Nuovo Cimento **63A** (1969) 892.
- 7) A. Kusumegi, M. Mishina, Y. Murata, K. Ukai, K. Ueno, T. Takahashi and S. Matsumoto, Nuovo Cimento **7A** (1972) 727.
- 8) P. Stichel and M. Scholz, Nuovo Cimento **34** (1964) 1381.
- 9) S. Costa, S. Ferroni, V. G. Gracco, E. Silva and C. Schaerf, Nuovo Cimento **45A** (1966) 696.

- 10) M. Beneventano, S. d'Angelo, F. de Notaristefani, P. Monacelli, L. Paoluzi, P. Persi, F. Sebastiani and M. Severi, *Nuovo Cimento* **15A** (1973) 449.
- 11) S. Iwata, *INS-TH* **64** (1970).
- 12) S. Fukui, T. Ohsuka, K. Ueno, Y. Inagaki, A. Sasaki, S. Iwata, A. Kusumegi, M. Mishina, T. Miyachi, I. Sato and K. Ukai, *Japan J. Appl. Phys.* **10** (1971) 1597.
- 13) Y. Inagaki, Y. Doi, M. Takamatsu, M. Mishina and A. Sasaki, *INS-report* **197** (1973).
- 14) H. Hinterberger and R. Winston, *Rev. sci. Instrum.* **37** (1966) 1094.
- 15) C. Chedester et al, *Phys. Rev.* **82** (1951) 958.
R. L. Martin et al, *Phys. Rev.* **82** (1952) 1052.
J. W. Cronin et al, *Phys. Rev.* **107** (1957) 1121.
T. Fujii, *Phys. Rev.* **113** (1959) 695.
A. G. Meshkovskii et al, *JETP* **10** (1960) 697.
R. M. Edelman et al, *Phys. Rev.* **122** (1961) 252.
M. P. Blandin et al, *JETP* **19** (1964) 279.
M. Crozon et al, *Nucl. Phys.* **64** (1965) 567.
G. Giacomelli et al, *CERN/HERA* **69-1** (1969).
F. Binon et al, *Nucl. Phys.* **B17** (1970) 168.
- 16) J. D. Jackson, *Nuovo Cimento* **34** (1964) 1644.
- 17) R. L. Walker, *Phys. Rev.* **182** (1969) 1729.
- 18) *Review of Modern Physics* **45**, No. 2, part II (1973).
- 19) D. Lüke and M. Scheunert, *Nuovo Cimento* **58** (1968) 234.
A. F. Meyer, *Nucl. Phys.* **B9** (1969) 244.
- 20) M. P. Locher and W. Sandhas, *Zeitschrift für Physik* **195** (1966) 461.
- 21) M. Jacob and G. C. Wick, *Annals of Physics* **7** (1959) 404.
- 22) A. A. Zayats, *Soviet J. of Nucl. Phys.* **13** (1971) 615.
- 23) J. B. Blatt and V. F. Weisskopf, in *Theoretical Nuclear Physics*, (John Wiley & Sons, New York, London) p. 796.
- 24) K. Ueno, Thesis for Nagoya University (unpublished).